Journal of Medicinal Chemistry



Article

# Optimization of Novel Indazoles as Highly Potent and Selective Inhibitors of Phosphoinostide-3-Kinase Delta for the Treatment of Respiratory Disease

Kenneth David Down, Augustin Amour, Ian R Baldwin, Anthony W.J. Cooper, Angela M Deakin, Leigh M Felton, Stephen B Guntrip, Charlotte Hardy, Zoë A Harrison, Katherine L. Jones, Paul Jones, Suzanne E Keeling, Joelle Le, Stefano Livia, Fiona Lucas, Christopher J Lunniss, Nigel J Parr, Ed Robinson, Paul Rowland, Sarah Smith, Daniel A Thomas, Giovanni Vitulli, Yoshiaki Washio, and Nicole Hamblin

*J. Med. Chem.*, **Just Accepted Manuscript** • DOI: 10.1021/acs.jmedchem.5b00767 • Publication Date (Web): 24 Aug 2015



## Just Accepted



ACS Publications

Journal of Medicinal Chemistry is published by the American Chemical Society. 1155 Sixteenth Street N.W., Washington, DC 20036

# Optimization of Novel Indazoles as Highly Potent and Selective Inhibitors of Phosphoinositide 3-Kinase Delta for the Treatment of Respiratory Disease

*Kenneth Down[$], Augustin Amour[$], Ian R. Baldwin[†], Anthony W. J. Cooper[$], Angela M. Deakin[¦], Leigh M. Felton[‡], Stephen B. Guntrip[$1], Charlotte Hardy[$], Zoë A. Harrison[$], Katherine L. Jones[‖], Paul Jones[$], Suzanne E. Keeling[$], Joelle Le[#], Stefano Livia[$], Fiona Lucas[$], Christopher J. Lunniss[$], Nigel J. Parr[‖], Ed Robinson[$], Paul Rowland[†], Sarah Smith[^], Daniel A. Thomas[^], Giovanni Vitulli[$], Yoshiaki Washio[†], J. Nicole Hamblin[$,]**

[$]Refractory Respiratory Inflammation DPU, and [¦]Allergic Inflammation DPU, Respiratory Therapeutic Area, GlaxoSmithKline R&D, Gunnels Wood Road, Stevenage, SG1 2NY, UK.

[†]Molecular Discovery Research, [^]Biological Sciences, and [#]Computational Chemistry, Platform Technology & Science, GlaxoSmithKline R&D, Gunnels Wood Road, Stevenage, SG1 2NY, UK.

[‡]Experimental Medicine Unit, and [‖]Epinova DPU, ImmunoInflammation Therapeutic Area, GlaxoSmithKline R&D, Gunnels Wood Road, Stevenage, SG1 2NY, UK.

[1]Present addess: Argenta Discovery, Harlow, Essex, CM19 5TR, UK.

Abstract

Optimisation of lead compound **1**, through extensive use of structure-based design and a focus on PI3Kδ potency, isoform selectivity and inhaled PK properties, led to the discovery of clinical candidates **2** (GSK2269557) and **3** (GSK2292767) for the treatment of respiratory indications *via* inhalation. Compounds **2** and **3** are both highly selective for PI3Kδ over the closely related isoforms and are active in a disease relevant Brown Norway Rat acute OVA model of Th2-driven lung inflammation.

## Introduction

Phosphoinositide 3-kinase delta (PI3Kδ) is a lipid kinase belonging to the Class 1 PI3K family, along with the closely homologous isoforms α, β and γ.[1,2] This family of enzymes catalyzes the phosphorylation of phosphatidylinositol-4,5-bisphosphate to produce the key signalling molecule phosphatidylinositol-3,4,5-triphosphate triggering a series of downstream biological events that ultimately impact on cell growth, proliferation, chemotaxis, differentiation and survival.[3,4,5]

PI3Kδ is highly enriched in leukocytes, making it an attractive target for the treatment of inflammatory conditions, such as asthma[6], chronic obstructive pulmonary disease[7] (COPD) and autoimmune diseases.[8] Furthermore, both PI3Kδ knock-out and kinase dead knock-in mice are viable and have a phenotype consistent with immunological effects on B-cells, T-cells and neutrophils.[9] PI3Kγ is also a reported target in inflammatory disease[10] and mutagenic mice are again viable, however PI3Kα and β knock-out mice are embryonically lethal, indicating the importance of subtype specific inhibitors for therapeutic intervention.[9] Targeting PI3Kδ is also of high interest for oncology indications, such that

GS-1101 (idelalisib, formally Cal-101)[11] has recently been approved for the treatment of patients with relapsed chronic lymphoid leukemia and non-Hodgkin lymphoma.

Herein we describe the medicinal chemistry program, starting from compound **1**, that ultimately led to the discovery of two inhaled clinical candidates GSK2269557 (**2**) and GSK2292767 (**3**) (Fig. 1) for the treatment of respiratory diseases such as asthma and COPD.

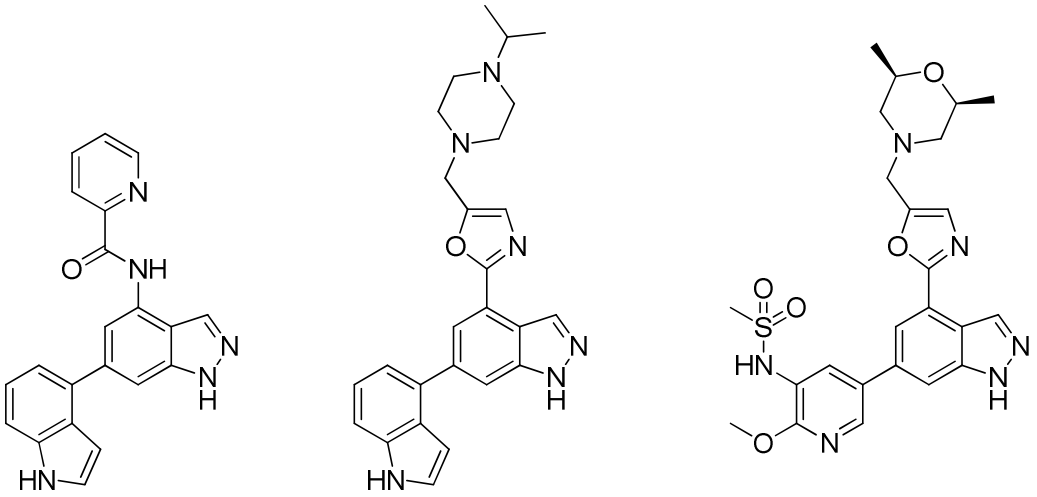

**1** **2** **3**

**Figure 1.** Structures of **1**, **2** and **3.**

## Results and Discussion

Compound **1** was a potential lead molecule that was discovered via SAR investigation against an un-related kinase, triggered by data from kinase cross-screening[12] (manuscript in preparation). We selected compound **1** as a lead due to its promising selectivity profile for PI3Kδ over the closely related PI3K isoforms, α, β and γ (Table 1). Given the critical role of PI3Kδ in immune responses and keen at the inception of this work to avoid any potential negative impact of broad systemic inhibition of this

biology, we embarked upon a lead optimization program with the aim of delivering an inhaled clinical candidate.

We set ourselves a challenging target profile, such that throughout the optimization program we focused on achieving compounds that had:

- High selectivity (>100 fold) for PI3Kδ over its related isoforms (α, β and γ)
- High cellular potency ($pIC_{50} > 9$)
- Moderate to high intrinsic clearance and low oral bioavailability

Inhibition of PI3K enzymatic activity was determined using a homogeneous time resolved fluorescence (HTRF) assay format.[13] As well as PI3K isoform selectivity we also sought compounds that were selective over the wider kinome and we obtained this data on selected compounds using available in-house and external assays. To measure cellular activity for compounds of interest, a peripheral blood mononuclear (PBMC) assay was adopted using cytostim to stimulate cytokine production from the T-lymphocyte compartment. Interferon gamma (IFNγ) was selected as an optimal analyte owing to robust stimulation by cytostim and exquisite sensitivity to PI3Kδ inhibition. We required high potency in this assay in order to minimize the required dose for inhaled delivery. The target PK profile was intended to minimize systemic circulation after inhaled delivery; moderate to high intrinsic clearance in order to ensure removal of drug once absorbed through the lung and low oral bioavailability to limit absorption of the swallowed fraction of the inhaled dose.[14]

We chose to explore the SAR at the two positions of substitution on the indazole core. To begin with, a set of 4-position amide modifications were prepared whilst keeping the 6-indole substituent fixed. The results are summarized in Table 1. Phenyl analogue **4** showed an approximate 10-fold drop in potency compared to compound **1**, indicating the potential importance of the *ortho* heteroatom. This was

substantiated by thiazole analogue **5** and 2-methylpyrazole analogue **6**, both of which displayed similar potency and selectivity to compound **1**. We postulated that this may be due to an internal hydrogen bond that maintains the planarity of the amide and thus enhances the stability of the preferred binding conformation. Wanting to probe this further and due to the lack of a suitable crystal structure of PI3Kδ at this time, a homology model was built to enable structure-based design and aid the rationalization of SAR.[15] The model (Fig. 2) suggested that the planar conformation of the amide allows the compounds to be accommodated under the glycine rich loop in the vicinity of bulky residues Met752 and Trp760. The apparent requirement for planarity was further investigated by methylation of the amide nitrogen atom to give compound **7** which caused a greater than 100-fold reduction in potency. The 1-methylpyrazole analogue **8** and the 1-isopropylpyrazole analogue **9** demonstrated a 10-fold drop in potency compared to compound **6** further corroborating the hypothesis that a planar amide conformation was important for potency.

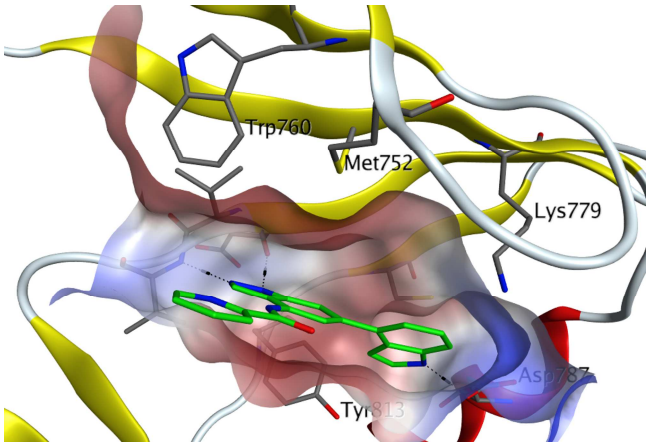


**Figure 2.** Compound **1** docked into a PI3Kδ homology model[15] displaying the planarity of the amide. Coloured shading represents a lipophilic (brown), neutral (white) or hydrophilic (blue) region of the

protein surface. Hydrogen bonds are highlighted with dashed lines between the indazole and the hinge region (Val828) and the indole and Asp787.

Methylation of compounds **1** and **5** to give compounds **10** and **11**, respectively, gave an increase in potency and selectivity that indicated an interesting lipophilic vector to pursue. In contrast, 5-methylpyridine analogue **12** showed no increase in potency compared to compound **1**, indicating the specificity of the substitution vector. More importantly, this initial SAR exploration suggested that PI3Kδ potency could be increased without substantially increasing the potency of the related isoforms, for instance the selectivity of compound **11** was approximately 100-fold or better against PI3Kα, β and γ.

**Table 1.** 4-Position amide modifications to give compounds **4** – **12**.

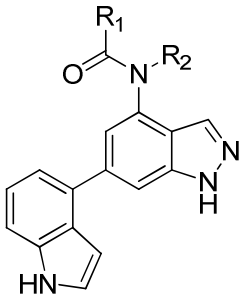


| Cmpd | $R_1$ | $R_2$ | $pIC_{50}$[a] PI3Kδ | PI3Kα | PI3Kβ | PI3Kγ |
|---|---|---|---|---|---|---|
| **1** | 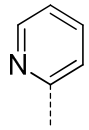 | H | 7.0 ± 0.14 (5) | 5.0[b] ± 0.10 (4) | 5.2 ± 0.25 (4) | 5.2[c] ± 0.11 (5) |
| **4** | 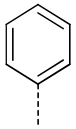 | H | 5.9 ± 0.13 (3) | <4.6 (2) | 4.7[c] (2) | 4.9[c] ± 0.04 (3) |

| | | | | | | |
|---|---|---|---|---|---|---|
| **5** | 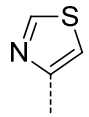 | H | 6.8 ± 0.20 (4) | <4.6 (3) | 4.9 ± 0.16 (3) | 5.0 ± 0.15 (4) |
| **6** | 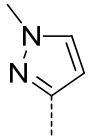 | H | 7.0 ± 0.11 (4) | <4.6 (3) | 4.9[c] ± 0.07 (4) | 5.0[b] ± 0.12 (4) |
| **7** | 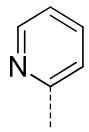 | Me | 4.8 (1) | <4.6 (1) | <4.6 (1) | <4.6 (1) |
| **8** | 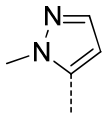 | H | 6.1 ± 0.11 (6) | <4.6 (6) | 4.7[c] ± 0.04 (5) | 4.7 ± 0.04 (5) |
| **9** | 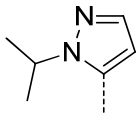 | H | 6.0 ± 0.23 (3) | <4.6 (3) | 4.6[b] (3) | 4.7[c] ± 0.07 (3) |
| **10** | 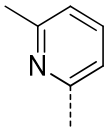 | H | 7.8 ± 0.09 (6) | 4.7[c] ± 0.06 (4) | 5.5 ± 0.05 (4) | 6.1 ± 0.08 (5) |
| **11** | 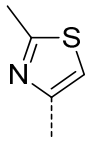 | H | 7.3 ± 0.24 (7) | <4.6 (3) | 5.0 ± 0.04 (3) | 5.4[c] ± 0.11 (7) |
| **12** | 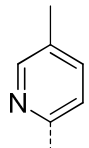 | H | 6.9 ± 0.07 (2) | <4.6 (2) | 4.8 ± 0.06 (2) | 5.9 ± 0.02 (2) |

[a]Mean ± SEM (number of test occasions). [b]Tested <4.6 on 2 occasions. [c]Tested <4.6 on 1 occasion.

To assess the suitability of the series for inhaled delivery *in vitro* clearance data in rat microsomes and subsequently *in vivo* pharmacokinetic data from Sprague Dawley male rats was obtained. Compounds

were administered by the oral or intravenous routes, at a dose level of 3 and 1mg/kg respectively (n=2 rats/route). As well as the good correlation between *in vitro* and *in vivo* clearance (Table 2), an interesting correlation between the torsion angle of the amide (Fig. 3) and the *in vivo* stability of the series was observed, such that increasing the torsion angle (e.g. compounds **6** to **8** to **9**) resulted in decreased clearance and increased bioavailability. This data implied that amide hydrolysis was a key metabolic pathway and we were subsequently able to demonstrate this by spiking with the resultant amine during the analysis of the PK samples. Pleasingly, moderate-to-high clearance and low oral bioavailability were observed for preferred compounds **6**, **10** and **11**, suggesting that maintaining the planarity of the amide was beneficial not only for potency but also for the intended PK profile. Kinetic solubility was measured using a high throughput assay with chemiluminescent nitrogen detection (CLND)[16]. Compounds **10** and **11** both displayed low solubility (2 and 12μg/ml, respectively).

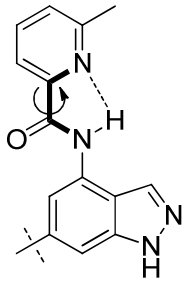

**Figure 3.** Torsion angle of the amide bond.

**Table 2.** Amide torsion angle and pharmacokinetic data for selected compounds.

| Cmpd | *In vitro* metabolism (ml/min/g liver)[a] | $Cl_b$ (ml/min/kg)[b] | F%[b] | Amide torsion angle (degrees)[c] |
|---|---|---|---|---|
| **6** | NR | 36 | 1 | 0 |
| **8** | 2 | 16 | 19 | 14 |
| **9** | <1 | 9 | 29 | 23 |

| | | | | |
|---|---|---|---|---|
| **10** | 11 | 49 | 2 | 0 |
| **11** | 6 | 28 | 2 | 0 |

[a]Compounds were tested for metabolic stability in rat microsomes at a concentration of 0.5μM in the incubation. [b]Compounds were tested in Sprague Dawley male rats and were administered discretely by the oral and intravenous routes, at a dose level of 3 and 1mg/kg respectively (n=2 rats/route). [c]Dihedral angle after optimization at the DFT-B3LYP/6-31G** level of theory.

We next switched our attention to the 6-position of the indazole template in search of further enhancement of potency and selectivity. Keeping the methyl thiazole amide of compound **11** in place, an array of compounds was synthesized which are summarized in Table 3.

**Table 3.** 6-Position indole modifications to give compounds **13** – **21**.

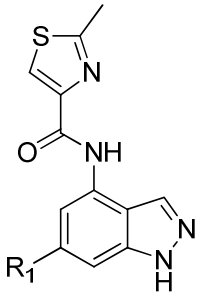


| Cmpd | $R_1$ | $pIC_{50}$[a] PI3Kδ | PI3Kα | PI3Kβ | PI3Kγ | clogP[b] |
|---|---|---|---|---|---|---|
| **11** | 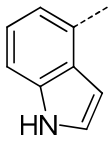 | 7.3 ± 0.24 (7) | <4.6 (3) | 5.0 ± 0.04 (3) | 5.4[c] ± 0.11 (7) | 4.1 |
| **13** | 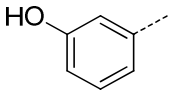 | 6.5 ± 0.08 (2) | 4.8 ± 0.07 (2) | 5.1 ± 0.02 (2) | 4.9 ± 0.13 (2) | 3.5 |

| | | | | | | |
|---|---|---|---|---|---|---|
| **14** | 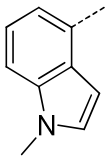 | 5.3 ± 0.04 (4) | <4.6 (4) | <4.6[d] (4) | <4.6 (4) | 4.6 |
| **15** | 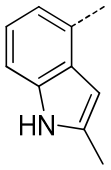 | 7.7 ± 0.10 (5) | 5.1[c] ± 0.08 (5) | 5.5 ± 0.05 (5) | 5.5 ± 0.15 (5) | 4.6 |
| **16** | 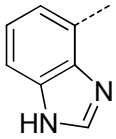 | 6.5 (1) | <4.6 (1) | <4.6 (1) | <4.6 (1) | 3.6 |
| **17** | 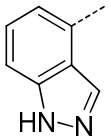 | 6.5 ± 0.08 (5) | <4.6 (7) | <4.6 (5) | 5.2 ± 0.19 (5) | 3.6 |
| **18** | 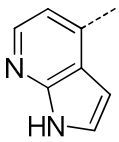 | 8.1 ± 0.10 (8) | 5.1 ± 0.06 (12) | 5.3[c] ± 0.06 (12) | 6.6 ± 0.06 (8) | 3.2 |
| **19** | 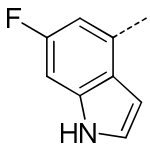 | 7.8 ± 0.09 (10) | 4.9 ± 0.03 (12) | 5.5 ± 0.06 (11) | 5.5 ± 0.09 (10) | 4.4 |
| **20** | 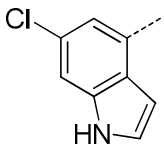 | 8.1 ± 0.12 (5) | 5.3 ± 0.08 (5) | 6.0 ± 0.03 (5) | 5.4 ± 0.06 (5) | 5.0 |
| **21** | 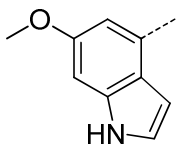 | 7.9 ± 0.10 (4) | 5.2 ± 0.10 (4) | 5.6 ± 0.05 (4) | 5.1 ± 0.05 (4) | 4.2 |

[a]Mean ± SEM (number of test occasions). [b]Calculated using Biobyte Version 4.0.[17] [c]Tested <4.6 on 1 occasion. [d]Tested 4.7 on 1 occasion.

*Meta*-phenol analogue **13** showed a loss of potency relative to compound **11** and this observation held true for all of the mono-cyclic indole replacements we prepared. *N*-Methyl indole analogue **14** showed a dramatic 100-fold loss of potency. Examination of the docking model (Fig. 4) suggests steric constraints in this region of the binding site and also that a potentially important H-bond interaction to Asp787 might be disrupted. 2-Methylindole analogue **15** was predicted by modeling to fill a small lipophilic pocket and gave a small increase in potency, albeit at the price of an increase in lipophilicity. Benzimidazole analogue **16** and indazole analogue **17** showed reduced potency relative to compound **11**, potentially due to reduced H-bond donating ability compared to the indole or maybe as a consequence of introducing polarity into a lipophilic pocket. 7-Azaindole analogue **18** displayed an 8-fold increase in potency, however the PI3Kγ potency also increased and this was indicative of poor wider kinase selectivity later discovered for this compound. This could potentially be explained by the ability of the 7-azaindole to act as a hinge-binder itself, allowing compound **18** to adopt different binding conformations across the human kinome. Modeling suggested substitution in the 6-position of the indole looked feasible and indeed, incorporation of fluorine (**19**), chlorine (**20**) or methoxy (**21**) substituents all increased potency whilst maintaining the selectivity profile over the other isoforms. However, compound **20** also had increased lipophilicity compared to compound **11**, so we did not see any advantage in using this group in subsequent compounds and, whilst compounds **19** and **21** did not substantially increase lipophilicity, they still did not achieve our target potency.

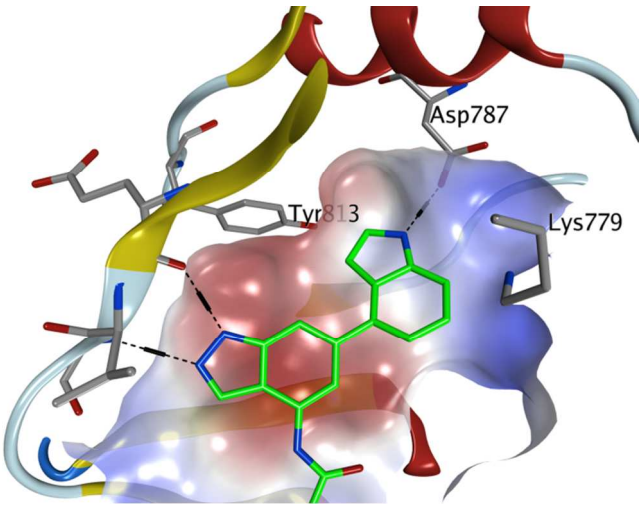


**Figure 4.** Close-up of the hinge and back pocket region of compound **1** docked in PI3Kδ. Hydrogen bonds are highlighted with dashed lines. Coloured shading represents a lipophilic (brown), neutral (white) or hydrophilic (blue) region of the protein surface.

Unable to significantly improve on the indole moiety at the 6-position of the indazole template, we turned our attention back to the 4-position. Careful re-evaluation of SAR, coupled with closer examination of compounds modeled into PI3Kδ, indicated that there was potentially space to substitute on the heteroaryl ring to search for further interactions. Table 4 summarizes our efforts in the area. Unable to differentiate between compounds **10** and **11**; extended compounds with both the pyridyl and thiazole heteroaryl groups in place were prepared.

**Table 4.** Heteroaryl amide substitutions to give compounds **22** – **29**.

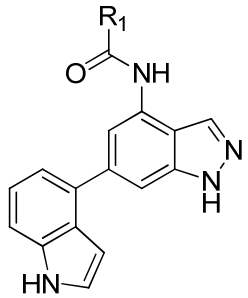

| Cmpd | $R_1$ | $pIC_{50}$[a] PI3Kδ | PI3Kα | PI3Kβ | PI3Kγ |
|---|---|---|---|---|---|
| **11** | 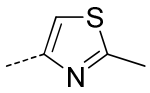 | 7.3 ± 0.24 (7) | <4.6 (3) | 5.0 ± 0.04 (3) | 5.4[b] ± 0.11 (7) |
| **22** | 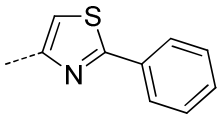 | 6.3 ± 0.03 (2) | <4.3 (1) | 4.9 ± 0.24 (2) | 5.1 ± 0.38 (2) |
| **23** | 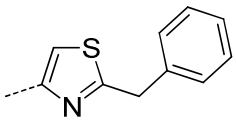 | 7.1 ± 0.26 (2) | <4.6 (1) | <4.6 (2) | 4.9[b] (2) |
| **24** | 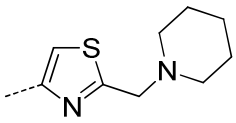 | 8.0 ± 0.16 (7) | 4.7[b] ± 0.03 (3) | 4.8 ± 0.04 (3) | 4.8[b] ± 0.08 (6) |
| **25** | 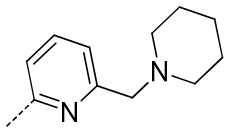 | 7.9 ± 0.07 (14) | <4.6 (18) | 4.9[c] ± 0.04 (16) | <4.6 (16) |
| **26** | 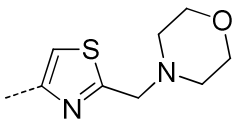 | 8.2 ± 0.07 (8) | 5.0[d] ± 0.04 (8) | 5.1[be] ± 0.08 (8) | 5.5 ± 0.06 (10) |
| **27** | 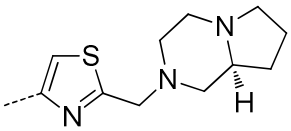 | 8.4 ± 0.03 (5) | 5.1 ± 0.04 (6) | 5.1 ± 0.03 (5) | 5 ± 0.09 (5) |

| | | | | | |
|---|---|---|---|---|---|
| **28** | 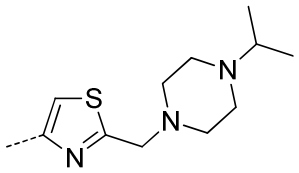 | 8.5 ± 0.01 (2) | 5.9 ± 0.01 (2) | 5.8 ± 0.03 (2) | 5.4[b] ± 0.07 (3) |
| **29** | 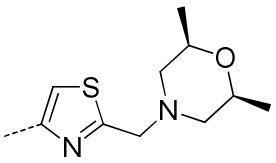 | 8.7 ± 0.08 (7) | 4.9 ± 0.05 (8) | 5.3 ± 0.05 (8) | 5.6 ± 0.12 (9) |

[a]Mean ± SEM (number of test occasions). [b]Tested <4.6 on 1 occasion. [c]Tested <4.6 on 3 occasions. [d]Tested <4.6 on 2 occasions. [e]Tested <5.2 on 1 occasion.

Adding further aromatic rings in this region did not enhance potency. For instance, changing the methyl substituent of compound **11** to phenyl (to give compound **22**) reduced potency 10-fold, whilst benzyl substituted analogue **23** was equipotent, despite the large molecular weight increase. A piperidine substituent on the methyl group of compounds **10** and **11** to give compounds **24** and **25**, respectively, showed an increase in potency whilst also enhancing the selectivity. However compound **25**, was significantly more active in a hERG binding assay ($pIC_{50}$ 6) than compound **24** ($pIC_{50}$ <4.3), a trend that was repeated with other extended pyridyl analogues in the series. For that reason subsequent compounds focused on maintaining the thiazole group. There was little difference in potency or selectivity between piperidine analogue **24** and morpholine analogue **26** in this region and bicyclic amines could also be introduced (such as compound **27)** suggesting that moderation of the lipophilicity and basicity of the compounds in this region was achievable, without drastically altering the potency and selectivity profile. Compound **26** displayed good potency ($pIC_{50}$ 7.8) in the PBMC assay, albeit below our stated target, low CLND solubility (8μg/ml) and high i*n vitro* clearance (11ml/min/g) in rat microsomes.

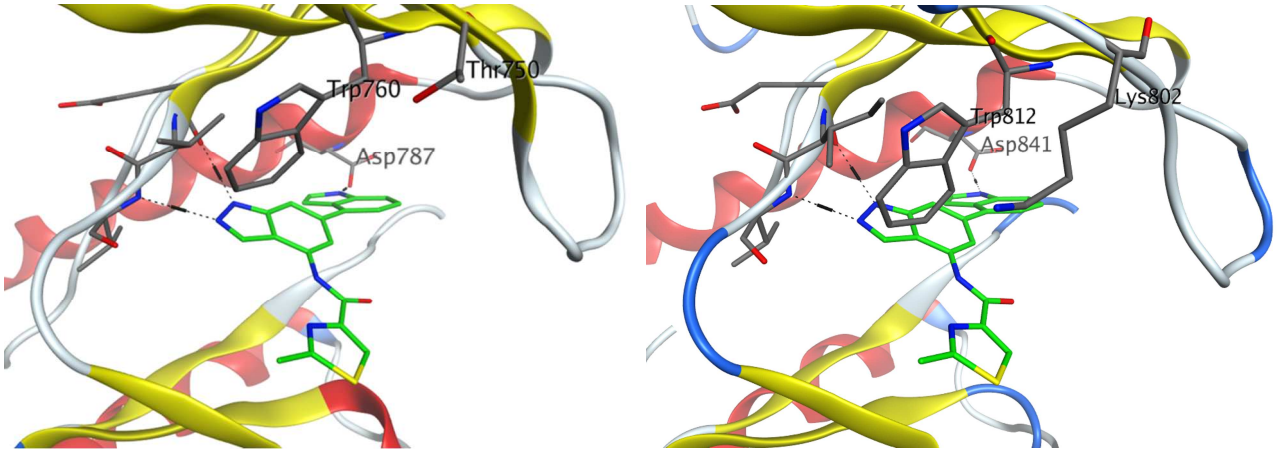


**Figure 5.** Comparison of PI3Kδ (left) and PI3Kγ (right) with compound **11** docked in to the active site, highlighting the different residue aligned adjacent to the conserved tryptophan (Thr750 for PI3Kδ and Lys802 for PI3Kγ). Hydrogen bonds are highlighted with dashed lines.

On further examination of the modeling we hypothesized that the lipophilic basic amine, which is predicted to be charged at physiological pH, would align next to Trp760 (conserved in PI3Kα, β and γ), forming a charge to pi-electron cloud interaction. This interaction is accessible in PI3Kδ due to the fact that the residue adjacent to Trp760 is Thr750. However in PI3Kα, β and γ the residue adjacent to the Trp is Arg, Lys and Lys, respectively (shown for PI3Kγ in Fig. 5), and we speculated that these larger residues could clash with the bulky cyclic amine group. This would preclude the compounds from adopting the same binding mode in these PI3K isoforms compared to PI3Kδ and explains the enhanced potency increase for PI3Kδ over α, β and γ. This region of the protein is solvent exposed which allows the compounds still to bind in PI3Kα, β and γ. This Trp760 interaction has been recently reported by Sutherlin *et al.* for an unrelated series of PI3Kδ inhibitors[18].

To take advantage of this hypothesis we next prepared compounds with additional bulk around the pendant amine, hoping to drive potency and selectivity further and compounds **28** and **29** were indeed highly potent and exquisitely selective. They were also highly potent in the PBMC assay ($pIC_{50}$ 8.5 (n=5) and 8.7 (n=8), respectively) and had increased CLND solubility (83 and 20µg/ml, respectively) compared to compound **26**. The wider kinase selectivity profiles of both compounds were encouraging, with only ALK5 potency ($pIC_{50}$ 7) within 100-fold of compound **28** in a panel of 20 kinases and compound **29** was greater than 100-fold selective across all kinases in a similar panel[19]. However these compounds did not reach our stated potency goal and therefore we continued our exploration of the SAR.

We next hypothesized that we could potentially access a more direct route to this important Trp760 interaction using a heterocycle (exemplified in Fig. 6), thereby reducing the size of the compounds. Building on our hypothesis from the amide series that planarity may be required for potency we prepared a series of 5-membered heteroaryl groups. These compounds are summarized in Table 5.

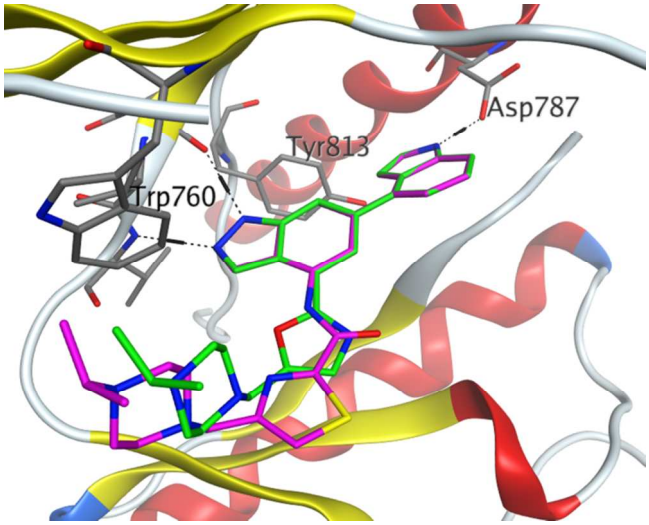

**Figure 6.** Overlay of compound **28** (pink) and compound **2** (green) docked in the PI3Kδ homology model, highlighting the more direct route to access the selectivity pocket adjacent to Trp760. Hydrogen bonds are highlighted with dashed lines.

Whilst the potency range amongst the heteroaryl groups was narrow, trends did emerge to guide subsequent compound design. Oxazole analogue **30** demonstrated good potency for PI3Kδ, on a par with compound **11**, albeit with reduced selectivity. Addition of methyl groups to the oxazole in either the 4- or 5-position (compounds **31** and **32**, respectively) had no significant impact on potency or selectivity. Oxadiazole analogue **33** displayed similar potency and selectivity to oxazoles **30** – **33** and *in vitro* rat microsomal stability was 7ml/min/kg, demonstrating that removal of the amide to directly attach the heteroaryl had not impacted on the target profile of high intrinsic clearance. Compounds **30** – **34** suggested that the H-bond donor of the amides was not necessary for potency and the presence of an H-bond acceptor could be sufficient to maintain potency. However, furan analogue **34** was equipotent to compounds **31** and **33**, suggesting that the H-bond acceptor (furan is at best only a very weak H-bond acceptor)[20] was also not necessary and we therefore assumed that the key driver for potency was maintaining the planarity of the heteroaryl ring. In order to probe our hypothesis further we prepared thiophene analogue **35**, predicted to have a non-planar preferred conformation, and this was 10-fold less potent than the oxygen containing heterocycles. Further supporting our hypothesis, methyl-substituted thiazole analogues **36** and **37** recovered some potency relative to compound **35**, presumably as some planarity was reintroduced, however these compounds were still inferior to the oxazole and oxadiazole.

**Table 5**. Heteroaryl amide replacements to give compounds **30** – **37**.

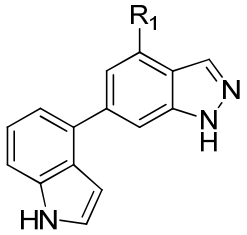

| Cmpd | $R_1$ | $pIC_{50}$[a] PI3Kδ | PI3Kα | PI3Kβ | PI3Kγ |
|---|---|---|---|---|---|
| **11** | 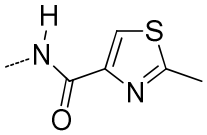 | 7.3 ± 0.24 (7) | <4.6 (3) | 5.0 ± 0.04 (3) | 5.4[b] ± 0.11 (7) |
| **30** | 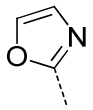 | 7.1 ± 0.21 (5) | 5.0[b] ± 0.10 (5) | 5.9 ± 0.04 (5) | 5.9 ± 0.11 (5) |
| **31** | 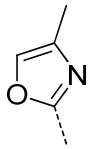 | 6.9 ± 0.14 (4) | 4.9 ± 0.05 (4) | 6.1 ± 0.08 (4) | 6.2 ± 0.12 (4) |
| **32** | 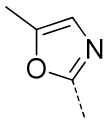 | 7.2 ± 0.13 (4) | 5.0 ± 0.07 (4) | 5.9 ± 0.13 (4) | 6.4 ± 0.12 (4) |
| **33** | 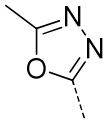 | 7.0 ± 0.21 (5) | <4.6[c] (5) | 5.5 ± 0.06 (5) | 5.9 ± 0.09 (5) |
| **34** | 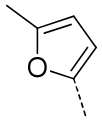 | 6.9 ± 0.38 (3) | 5.3 ± 0.14 (3) | 5.6 ± 0.22 (3) | 5.7 ± 0.13 (3) |
| **35** | 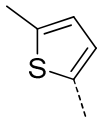 | 6.1 ± 0.11 (3) | 5.1 ± 0.08 (3) | 5.2 ± 0.33 (3) | 5.4 ± 0.17 (3) |
| **36** | 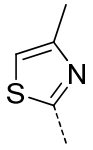 | 6.4 ± 0.19 (3) | <4.6[d] (3) | 5.2 ± 0.32 (3) | 5.6 ± 0.00 (2) |
| **37** | 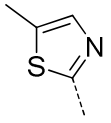 | 6.6 ± 0.21 (3) | 5.0 ± 0.14 (3) | 5.2 ± 0.21 (3) | 5.4 ±0.08 (3) |

[a]Mean ± SEM (number of test occasions). [b]Tested <4.6 on 1 occasion. [c]Tested 4.8 on 1 occasion. [d]Tested 5.5 on 1 occasion.

From these starting points we hoped that by addition of the groups previously identified to interact with the tryptophan we could improve the PI3Kδ potency above that of the other isoforms. Compounds with the extended amine on the oxadiazole and in both the 2- and 3-positions of the oxazole were prepared and are summarized in Table 6. Whilst compound **34** was useful for SAR purposes, the reported potential toxicological risks of furan dissuaded us from incorporating it into further compounds[21].

**Table 6.** Extended amine substitution on selected heteroaryl groups to give compounds **2** and **38** – **42**.

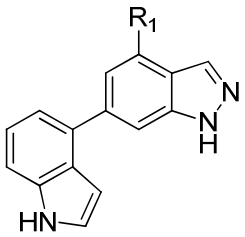


| | | pIC$_{50}$[a] | | | | | |
|---|---|---|---|---|---|---|---|
| Cmpd | $R_1$ | PI3Kδ | PI3Kδ p$K_i$[b] | PI3Kα | PI3Kβ | PI3Kγ | PBMC IFNγ |
| **38** | 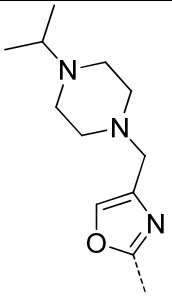 | 8.4 ± 0.00 (3) | - | 4.9[c] ± 0.03 (4) | 5.4 ± 0.10 (4) | 4.8 ± 0.02 (4) | 7.9 ± 0.22 (8) |
| **39** | 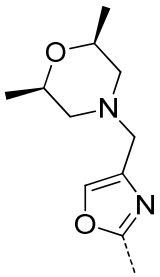 | 8.3 ± 0.02 (2) | - | 4.9 (1) | 5.9 ± 0.03 (2) | 5.6 ± 0.02 (2) | 7.1[d] ± 0.26 (8) |

| | | | | | | | |
|---|---|---|---|---|---|---|---|
| **40** | 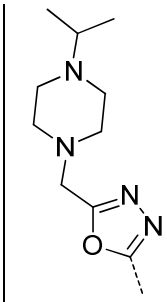 | 8.9[e] ± 0.05 (5) | - | 4.9 ± 0.09 (8) | 5.5 ± 0.11 (6) | 5.0 ± 0.04 (7) | 9.3[f] ± 0.30 (10) |
| **41** | 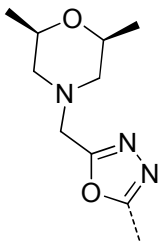 | 8.5[e] ± 0.19 (15) | - | <4.6[g] (17) | 6.0 ± 0.07 (17) | 5.7[a] ± 0.02 (15) | 8.3[f] ± 0.19 (13) |
| **2** | 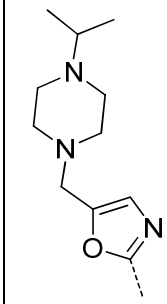 | - | 9.9 ± 0.09 (4) | 5.3[eh] ± 0.06 (29) | 5.8[e] ± 0.13 (27) | 5.2[i] ± 0.05 (33) | 9.7 ±0.21 (10) |
| **42** | 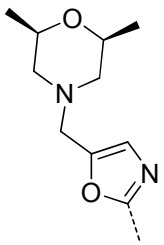 | 8.6 ± 0.06 (3) | - | 4.8 ± 0.09 (3) | 6.0 ± 0.08 (3) | 5.7 ± 0.08 (3) | 8.6[fj] ± 0.28 (12) |

[a]Mean ± SEM (number of test occasions). [b]The standard PI3Kδ assay was run at a 2mM ATP concentration. [c]Tested <4.6 on 2 occasions. [d]Tested >8.1 on 1 occasion. [e]Tested <4.6 on 1 occasion. [f]Tested >8.1 on 3 occasions. [g]Tested average of 4.7 on 4 occasions. [h]Tested <5.3 on 1 occasion. [i]Tested <4.6 on 3 occasions. [j]Tested >9.8 on 1 occasion and <6 one 1 occasion.

Oxazoles substituted in the 4-position with the preferred amines identified in compounds **28** and **29,** were thus prepared. Comparable potency and selectivity were obtained but, disappointingly compounds **38** and **39** were less active in the PBMC assay than their amide counterparts. Substituted oxadiazoles **40** and **41** had similar potency to compounds **28** and **29** and this activity translated to the PBMC assay. Compound **42**, an oxazole substituted in the 5-position, again showed similar potency in the enzyme and

PBMC assay to its amide analogue **29**. Oxazole compound **2**, however, was significantly more potent than its amide analogue **28** and the 4-substituted oxazole **38**, in both the enzyme and PBMC assays. The standard assay was modified to run at 2mM ATP concentration in order to be able to determine a pKi. These compounds confirmed our approach to successfully shortcut to the tryptophan interaction with an appropriate heterocycle.

Compounds **2** and **40** both met our original potency goal in the PBMC assay ($pIC_{50}$ >9) and had exquisite selectivity against the PI3K isoforms (Fig. 7; Concentration response plots for compound **2** in a modified HTRF assay). Both compounds **2** and **40** were also highly CLND soluble (110 and 118μg/ml, respectively), however compound **2** had marginally less potent hERG binding compared to compound **40** ($pIC_{50}$ 5.5 vs. 5.9, respectively) and, coupled with its higher PBMC potency, was selected for wider profiling to assess its potential as a clinical candidate.

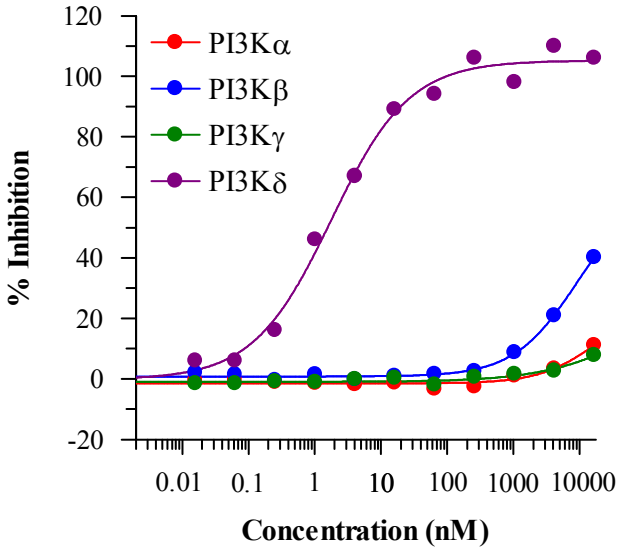


**Figure 7.** Concentration response plot of compound **2** against PI3Kα, β, γ and δ in a modified HTRF assay using an ATP concentration of 2 mM.[22] The data shown here are from a single experiment.

Wider kinase selectivity was impressive; compound **2** was greater than 1000-fold selective against the Millipore kinase panel (> 250 kinases in total).[23]

The rat PK profile of compound **2** was also encouraging but not ideal based on our stated goals. Low oral bioavailability (F 2%) was achieved and *in vivo* clearance of 28ml/min/kg, whilst lower than initially targeted, still met our criteria for progression. As well as being dibasic and moderately lipophilic (clogP 4.4), compound **2** also had a high volume of distribution of 6.3L/kg, which we hypothesized may lead to beneficial tissue retention properties when delivered to the lung.[24]

We progressed compound **2** to a human lung parenchyma assay wherein finely chopped lung tissue incubated with the plant lectin phytohaemagglutanin (PHA) for 72 hours induced production of cytokines including IFNγ and IL-2. This response was inhibited by compound **2** in a concentration-dependent manner, returning $pIC_{50}$ values of 8.2 (IFNγ) and 8.1 (IL-2).

In order to further investigate the hERG binding result, compound **2** was profiled in a rabbit cardiac ventricular wedge assay. Compound **2** induced concentration-dependent increases in QT interval and $T_{p-e}$ at 0.3 and 1μM (1 and 0.5 Hz) and an increase in QRS at 1μM (2 Hz), however, no treatment-related Torsades de Pointes (TdP) arrhythmias were observed in this study. A concentration of 1μM was calculated to be >300 fold above the predicted human free plasma $C_{max}$ at a therapeutic dose of 1 mg per day[25] and >150 fold higher than the lung parenchyma assay $pIC_{50}$. As we expected the delivered dose to be in the microgram rather than milligram range, we felt this risk was acceptably low.

In a disease relevant Brown Norway Rat acute OVA model of Th2 driven lung inflammation, compound **2** was shown to protect against eosinophil recruitment with an $ED_{50}$ of 67μg/kg (Fig. 8). The activity of compound **2** was also assessed using other endpoints in this model including, leukocyte recruitment to the lung (neutrophils, macrophages, CD4 and CD8 T-lymphocytes at 48 hours) and Th2

cytokines such as IL-13. Compound **2** dose-dependently reduced recruitment of all leukocyte subpopulations and IL-13 in the lungs.

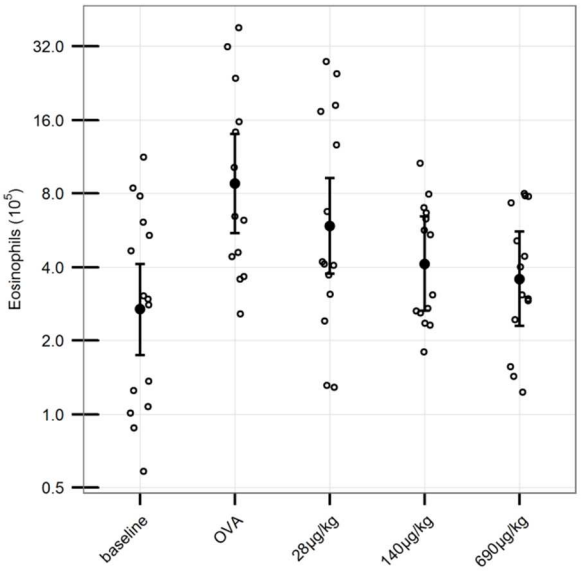


**Figure 8.** Inhibition of eosinophil recruitment by compound **2** in a rat acute OVA model. A trend test was constructed using analysis of variance which showed a significant decrease of eosinophil numbers with increasing concentrations of compound **2**. Prior to analysis the data from 2 experiments were standardised so that the average of the control groups were the same. The analysis of variance model used log eosinophil numbers as the response and the concentrations of compound **2** as a categorical factor along with the positive control of challenged, untreated animals. An $ED_{50}$ was calculated for compound **2** by using the 3 concentrations of compound **2**. In addition the positive (OVA challenge, no treatment) and negative controls (baseline, no challenge) were used to provide more information on the maximum and minimum responses for the model. The eosinophilic response was logged prior to fitting a 4 parameter logistic model to the data. The fitted curve was used to estimate the $ED_{50}$ along with its 95% confidence interval.

Based on this data, compound **2** was selected for progression to early clinical studies as a novel PI3Kδ inhibitor for the treatment or respiratory diseases by inhaled delivery.

Following the successful identification of a first inhaled candidate (compound **2**), we set out to identify a differentiated follow-up compound, with the combined aims of reducing residual hERG activity and increasing the *in vivo* clearance to minimize systemic exposure.

The classical hERG pharmacophore has been well described[26] and our approach to minimizing channel blockade focused on modulating the amine p$K_a$ and reducing lipophilicity. Compound **2** had a measured p$K_a$ of 8.1 and a clogP of 4.4. In our earlier work at the 4-position we had identified the morpholine group as a tolerated cyclic amine with reduced basicity; compound **41** for instance had a calculated p$K_a$ of 7.1, and so using this a starting point we turned our attention back to replacing the 6-position indole in order to reduce the lipophilicity. As previously discussed we had been unable to find a suitable replacement for the indole, however other internal PI3K programs[27] had since demonstrated success with a pyridine sulfonamide moiety (Fig. 9) and we looked to explore the utility of this group in our series, mindful of the need to maintain the exquisite selectivity and potency we had achieved with the indole group, whilst also targeting reduced lipophilicity. A range of compounds to explore this region by comparison to compound **11** were prepared, as summarized in Table 7.

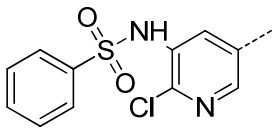


**Figure 9.** Pyridine sulfonamide moiety

**Table 7.** Exploration of the pyridine sulfonamide moiety to give compounds **43** – **50**.

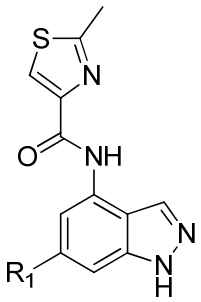

| | | pIC$_{50}$[a] | | | | | | |
|---|---|---|---|---|---|---|---|---|
| Cmpd | R1 | PI3Kδ | PI3Kα | PI3Kβ | PI3Kγ | PBMC IFNγ | clogP[b] | hERG |
| **11** | 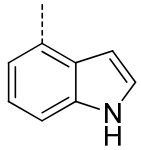 | 7.3 ± 0.24 (7) | <4.6 (3) | 5.0 ± 0.04 (3) | 5.4[c] ± 0.11 (7) | ---- | 4.1 | ---- |
| **43** | 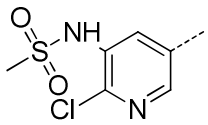 | 8.7 ±0.07 (12) | 6.5 ± 0.08 (16) | 6.0 ± 0.08 (16) | 7.3[d] ± 0.06 (16) | 7.2 ± 0.22 (3) | 2.3 | <4.3[i] (5) |
| **44** | 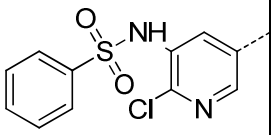 | 8.9 ± 0.12 (15) | 6.7 ± 0.13 (17) | 6.3[c] ± 0.12 (15) | 7.6 ± 0.19 (12) | 7.3[ef] ±0.11 (6) | 4.0 | <4.3 (2) |
| **45** | 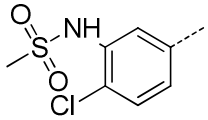 | 6.2 ± 0.09 (2) | 4.8 ± 0.01 (2) | 4.8 ± (0.04 (2) | 5.4 ± 0.06 (2) | ---- | 3.3 | 4.9 (1) |
| **46** | 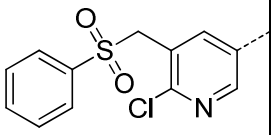 | 6.0 ± 0.00 (2) | 4.6[c] (2) | 4.7 ± 0.01 (2) | <4.6 (2) | 5.7 ± 0.09 (2) | 3.4 | 5.2 (2) |
| **47** | 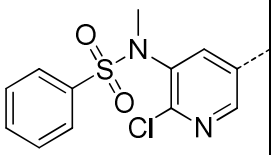 | 6.3 ± 0.08 (2) | <4.6 (2) | <4.6 (2) | <4.6 (2) | 5.9 ± 0.44 (3) | 3.8 | <4.3 (2) |
| **48** | 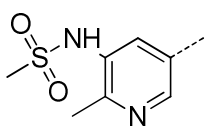 | 7.5[g] ± 0.27 (6) | 5.5[d] ± 0.07 (9) | 5.4[d] ± 0.05 (7) | 6.2 ± 0.10 (6) | 6.4 ± 0.13 (3) | 2.0 | 4.7 (1) |

| | | | | | | | | |
|---|---|---|---|---|---|---|---|---|
| **49** | | 7.1 ± 0.05 (8) | 5.1 ± 0.05 (8) | <4.6[h] (8) | 6.5 ± 0.05 (8) | 5.6 ± 0.12 (5) | 2.1 | 4.6 (2) |
| **50** | | 7.9 ± 0.03 (3) | 6.1 ± 0.08 (4) | 6.1 ± 0.08 (4) | 6.7 ± 0.11 (4) | 7.9 ± 0.15 (8) | 2.9 | 4.7 (1) |

[a]Mean ± SEM (number of test occasions). [b]Calculated using Biobyte Version 4.0.[17] [c]Tested <4.6 on 1 occasion. [d]Tested <4.6 on 2 occasions. [e]Tested <4.3 on 1 occasion. [f]Returned no value on 1 occasion. [g]Failed to return a value on 2 occasions. [h]Tested 4.58 on 1 occasion. [i]Tested 4.3 on 2 occasions.

Replacing the indole with a pyridine methylsulfonamide to give compound **43** resulted in a greater than 10-fold increase in potency for PI3Kδ. Compound **43** also had much reduced clogP compared to compound **11**. However, potency at the other PI3K isoforms was also significantly enhanced, such that compound **43** was no more selective than compound **11**. Phenyl sulfonamide **44** demonstrated no enhancement in potency compared to compound **43** and had the further disadvantage of a clogP similar to compound **11**. Both compounds **43** and **44** had similar PBMC potency with a drop of approximately 30-40 fold compared to the enzyme assay.

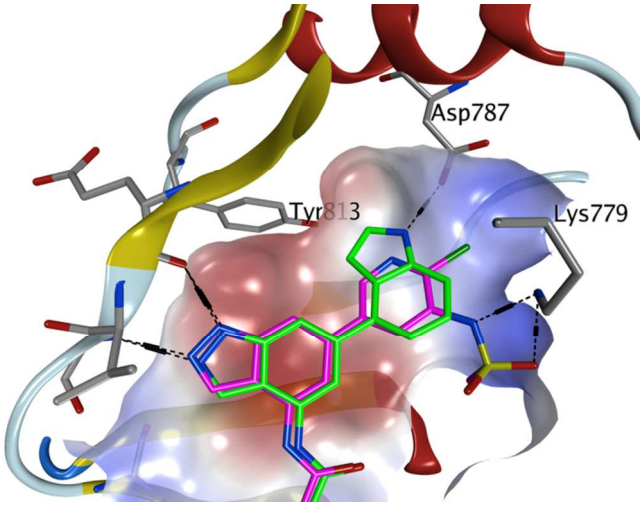

**Figure 10.** Overlay of docking of compounds **11** (green) and **43** (magenta), highlighting the differences between the interactions of the pyridine sulfonamide and the indole. Hydrogen bonds are highlighted with dashed lines.

We next sought to understand the key binding elements of the pyridine sulfonamide. Removing the pyridine nitrogen to give compound **45** resulted in a dramatic loss of potency. We hypothesized that the nitrogen would make an important interaction through water to backbone residues Tyr813 and Asp787. An overlay of compounds **11** and **43** (Fig. 10) showed the indole NH of compound **11** could be making a key H-bond interaction with the backbone, potentially displacing a water molecule with which the pyridine nitrogen of compound **43** interacts. We hypothesized that the indole would fit the lipophilic pocket better in this region but, as the pyridinesulfonamide was more potent, there were evidently multiple factors operating. To probe this further, we next prepared sulfone analogue **46** and *N*-methylsulfonamide analogue **47**. These two compounds showed a substantial drop in potency against all isoforms, suggesting the importance of the sulfonamide NH. Consideration of the binding site led us to postulate that the sulfonamide (measured p$K_a$ 6.4, thus predominantly ionized at physiological pH) would form a key charge-charge interaction with the conserved catalytic lysine (Lys779) and therefore, disruption of this lysine interaction in compounds **46** and **47** led to a drop in potency. The indole moiety was not hypothesised to interact with Lys779 and was thus a further explanantion for the enhanced potency of compound **43** over compound **11**. This also provided an explanation for the enhanced potency in the other PI3K isoforms which are homologous in this region.

To explore further the impact of sulfonamide ionization we investigated the effect of the *ortho*-pyridine substituent on potency. As well as moderating the p$K_a$ of the sulfonamide we postulated that changes in this region would also moderate the H-bond acceptor ability of the pyridyl nitrogen. Methyl

analogue **48** showed a greater than 10-fold potency drop against all isoforms and this was also reflected in a drop in the PBMC activity. Hydrogen analogue **49** caused a further small drop in the PI3Kδ potency which was not reflected in the other PI3K isoforms. However, the PBMC potency dropped a further 10-fold. Whilst we had potentially identified a useful indole replacement, the disappointing PBMC potency of those compounds was considered an issue. A breakthrough came when we introduced an *ortho*-methoxy group to give compound **50**. Although the PI3K potency of compound **50** was lower at all isoforms compared to compound **43**, compound **50** was actually more potent than compound **43** in the PBMC assay. We hypothesised that the lower p$K_a$ of the sulfonamide of compound **43** (measured as 6.4 vs 7.8 for compound **50**) was impacting on the PBMC potency (presumably through reduced cell permeation) despite the beneficial effect on PI3Kδ potency. We observed this trend across a number of compounds such that the lower the p$K_a$ of the sulfonamide, the greater the difference we saw between the PI3Kδ assay and the PBMC assay. Compound **50** also had a significantly lower clogP than compound **43**, thus confirming that we had successfully discovered an acceptable indole replacement with reduced lipophilicity, albeit reduced selectivity against the PI3K isoforms. hERG binding was low for compounds in Table 7, with only compound **46** above p$IC_{50}$ 5, however none of these compounds contained the extended basic amine.

Finally, we synthesised the fully elaborated compounds (Table 8) with a pendant morpholine in place based on the hypothesis that this could deliver the target selectivity. Compound **51**, the pyridine sulfonamide equivalent of compound **29**, demonstrated significantly enhanced potency both at the enzyme and in the PBMC assay, whilst also achieving high selectivity over the PI3K isoforms. Compound **3**, the pyridine sulfonamide analogue of compound **42,** was both highly potent in the enzyme and PBMC assay and highly selective over the PI3K isoforms. This addition of the amine had the same effect as described previously on PI3K isoform selectivity, such that compound **3** was greater than 500-

fold selective over the other PI3K isoforms. Compounds **3** and **51** both had reduced hERG binding compared to compound **2** ($pIC_{50}$ 5.5) but compound **3** had greater solubility and lower lipophilicity than compound **51** and therefore was selected for more extensive profiling to assess its potential as a clinical candidate.

**Table 8.** Fully elaborated compounds with a pyridine sulfonamide moiety to give compounds **3** and **51**.

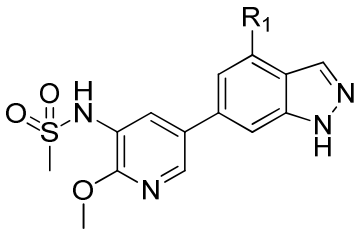

| | | $pIC_{50}$[a] | | | | | | | |
|---|---|---|---|---|---|---|---|---|---|
| Cmpd | R1 | PI3Kδ $pK_i$[b] | PI3Kα | PI3Kβ | PI3Kγ | PBMC IFNγ | clogP[c] | CLND solubility μg/ml | hERG |
| **51** | 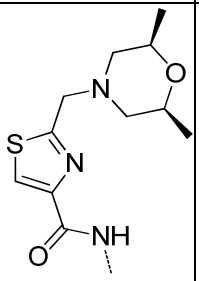 | 10.0 ± 0.07 (5) | 6.4 ± 0.04 (17) | 5.6 ± 0.09 (18) | 6.5 ± 0.05 (20) | 9.6 ± 0.20 (3) | 3.2 | 114 | 4.9 (3) |
| **3** | 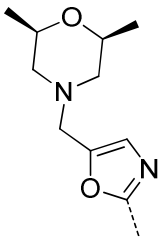 | 10.1 ± 0.02 (2) | 6.3 ± 0.07 (11) | 6.2 ± 0.06 (10) | 6.3 ± 0.10 (9) | 9.2 ± 0.09 (6) | 2.8 | 182 | 4.7 (6) |

[a]Mean ± SEM (number of test occasions). [b]The standard PI3Kδ assay was run at a 2mM ATP concentration. [c]Calculated using Biobyte Version 4.0[17].

Compound **3** was greater than 100-fold selective against a panel of in-house kinases[19] and in the Millipore panel[23] (>250 kinases in total).

In a human lung parenchyma assay, compound **3** inhibited both IFNγ and IL-2 production in a concentration-dependent manner, with $pIC_{50}$ values of 8.7 and 8.5, respectively.

In a rat PK study, the *in vivo* clearance of 50ml/min/kg for compound **3** was significantly higher than that for compound **2** and fitted well with our target profile for a follow-up inhaled candidate. The oral bioavailability was also low (F <2%), in line with the data observed for compound **2**.

In a rabbit cardiac ventricular wedge assay there was no effect on QT interval, $T_{p\text{-}e}$ or QRS and no significant risk of TdP arrhythmias over the concentration range tested (0.01-1μM), thereby demonstrating compound **3** had successfully mitigated the risk associated with compound **2**.

In the Brown Norway Rat acute OVA model of Th2 driven inflammation in the lungs of rats, compound **3** was shown to protect against eosinophil recruitment with an $ED_{50}$ of 35μg/kg, similar to compound **2**.

Given the differentiated pharmacokinetics of compound **3** along with its enhanced cardiovascular selectivity profile, this compound was selected as a back up to compound **2** for potential progression to early clinical studies.

Throughout the optimization process we made extensive use of computational modeling and subsequent to the medicinal chemistry program we were able to obtain a co-crystal structure of compounds **2** and **3** in a mouse PI3Kδ construct[28] (Fig. 11. See supplementary data for details). This structure showed that the modeling effectively predicted the observed binding mode with respect to the indazole and pyridinesulfonamide moieties, with only minor differences between the modeled and crystallized indole moiety. Crystallography also confirmed the planarity of the oxazole. We observed

some differences in the region containing the lipophilic amine of compound **2** such that the isopropyl group accessed the tryptophan, but we did not see the anticipated charge-pi cloud interaction between Trp760 and the piperazine. The position of the morpholine moiety of compound **3** was well predicted by the homology model and also overlaid well with the observed position of the piperazine in compound **2**, indicating that both amine moieties made a similar and important interaction with the protein.

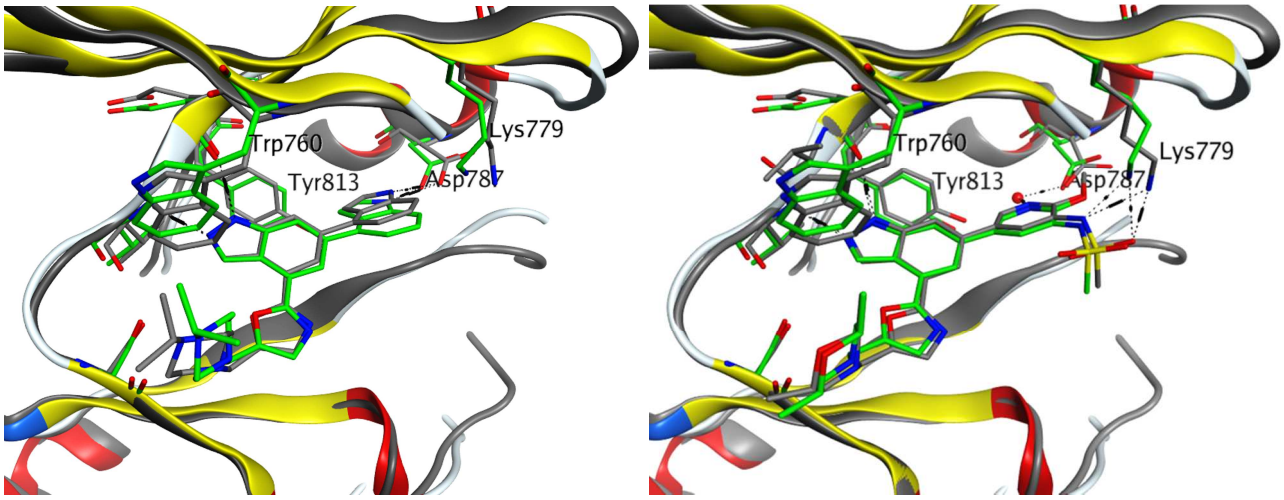


**Figure 11.** Compounds **2** (left) and **3** (right) co-crystallized in PI3Kδ (green), highlighting the differences in the tryptophan region compared to the modeled conformation (grey). Hydrogen bonds are highlighted in grey. The water (HOH403) mediated pyridine – Asp787 interaction is observed for compound **3**.

Our focus on obtaining the maximum potency for the lowest molecular weight was reflected well when we post-analyzed our data in ligand efficiency terms (Fig. 12).[29] The lead, compound **1**, has an LE of 0.37 and despite the significant changes made during optimization, compound **3** is very similar with an LE of 0.36. Compound **2** has an even higher LE of 0.41; collectively these data demonstrate effective compound growth during optimization.

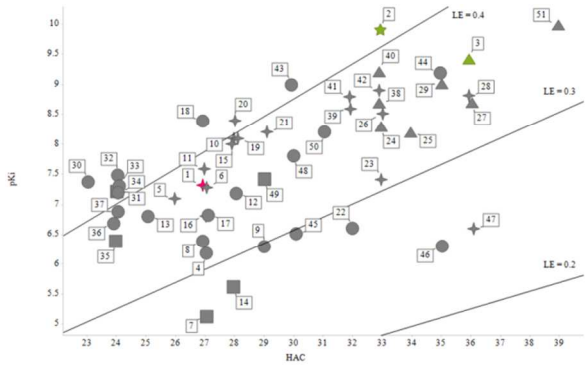


**Figure 12.** Heavy atom count (HAC) plotted against PI3Kδ pKi for compounds **1** – **51**, including compound **1** (pink) and compounds **2** and **3** (green). The lines drawn indicate constant LE as noted. Compounds are shaped by selectivity against the next nearest PI3K isoform: Square is 0-10 fold; circle is 10-100 fold; cross is 100-1000 fold; triangle is 1000-10000 fold; star is >10000 fold.

## Conclusion

We have described the discovery of potent and selective inhibitors of PI3Kδ as inhaled clinical compounds for the treatment of patients with respiratory disease. The optimization from a cross-screening hit through successive SAR iterations led to significant increases in potency and selectivity whilst achieving pharmacokinetic profiles within an ideal range for inhaled delivery.

## Chemistry

The compounds reported in this paper were prepared by a variety of methods from commercially available indazole compounds **53**, **54**, **55** and **56**.

Compounds prepared from compound **53** are described in Scheme 1.

Compound **53** was protected as the THP derivative **53i**, followed by Suzuki-Miyaura cross-coupling with indole-4-boronic acid to give compound **53ii**. Reduction of the nitro group gave amine **53iii** which was subjected to amide coupling using HATU with the appropriate carboxylic acid, followed by acid-catalyzed deprotection to give compounds **1**, **4**, **5**, **10**, **22**, **23** and **26**.

In a second variant of this reaction scheme, reduction of the nitro group of compound **53i** to give amine **53iv**, followed by amide coupling with 2-methylthiazole-5-carboxylic acid and HATU gave compound **53v**. This compound was converted to the boronic ester using a modified Miyaura borylation reaction to give the boronic ester **53vi**. Suzuki-Miyaura cross-coupling of compound **53vi** with the appropriate aryl halide followed by acid-catalyzed deprotection gave compounds **13**, **15**, **19-21** and **44** - **48**.

Finally, in a third variant of this scheme, compound **53** was subjected to a Suzuki-Miyaura cross-coupling to give compound **53vii**, followed by di-tosylation to give compound **53viii**. Reduction of the nitro group gave amine **53ix**, which was converted to iodide **53x** by treatment with diiodomethane, cuprous iodide, iodine and tert-butyl nitrite. Stille coupling with the appropriate stannane and deprotection using sodium hydroxide gave compounds **30** and **34**, **35**, **36** and **37**.

**Scheme 1.** Compounds prepared from compound **53**.

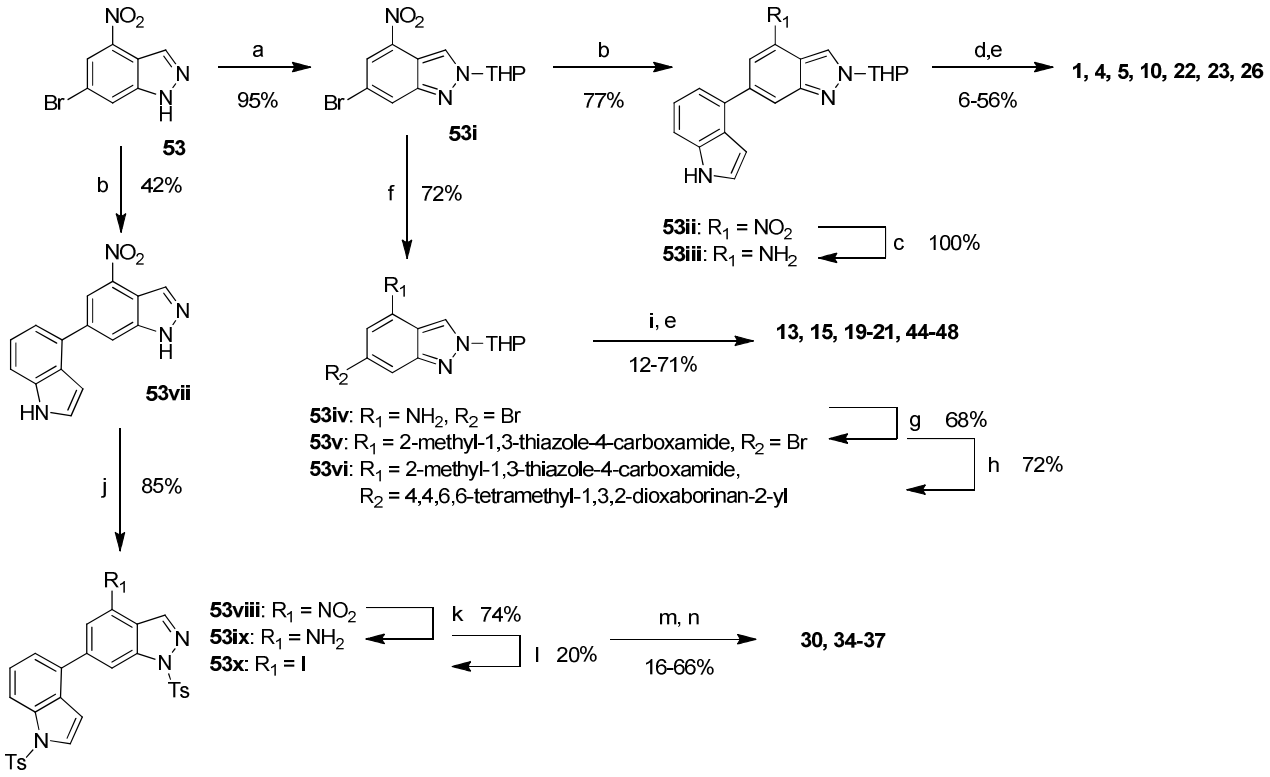


a) Dihydropyran, TFA, reflux; b) Indol-4-ylboronic acid, sat. $NaHCO_3$, $PdCl_2(dppf)$, IPA, 150°C, μW; c) 10% Pd/C, H-Cube®, 30bar $H_2$; d) R-$CO_2H$, HATU, DIPEA; e) SCX cartridge or 2M HCl or TFA or formic acid; f) Iron filings, $NH_4Cl$, ethanol/water, 80ºC; g) R-COCl, pyridine, DCM; h) 4,4,4',4',6,6,6',6'-octomethyl-2,2'-bi(1,3,2-dioxaborinane), KOAc, $PdCl_2(dppf)$, 1,4-dioxane, 80ºC; i) RX, 1,4-dioxane/water and either $PdCl_2(dppf)$, $Na_2CO_3$ or chloro(di-2-norbornylphosphino)(2'-dimethylamino-1,1'-biphenyl-2-yl)palladium(II), $K_3PO_4$; j) NaH, tosyl chloride, DMF; k) 10% Pd/C, $H_2$, EtOAc; l) $CH_2I_2$, $I_2$, CuI, t-butylONO; m) ArSn(n-butyl)$_3$, $Pd(PPh_3)_4$, DMF; n) 2M NaOH (aq), IPA.

Compounds prepared from compound **54** are described in Scheme 2.

Suzuki-Miyaura cross-coupling of compound **54** with an indole-4-ylboronic ester gave compound **54i** which was subjected to amide coupling using HATU and the appropriate carboxylic acid to give final compounds **6**, **8**, **9** and **12**.

In an alternative sequence, methylation of indazole **54,** using paraformaldehyde and sodium borohydride, gave compound **54ii** which underwent Suzuki-Miyaura cross-coupling with indole-4-boronic acid to give intermediate **54iii**. Amide coupling using HATU finally gave compound **7**.

Amide coupling of the starting material **54** with 2-methylthiazole-5-carboxylic acid and HATU gave compound **54iv** which could be reacted with *N*-methylindole-4-boronic acid to give compound **14**. A Suzkui-Miyaura cross-coupling of **54iv** with (2,3-diaminophenyl)-4-boronic acid gave **54v** which was converted to **16** by heating to reflux with triethylorthoformate in DMF.

**Scheme 2.** Compounds prepared from compound **54**.

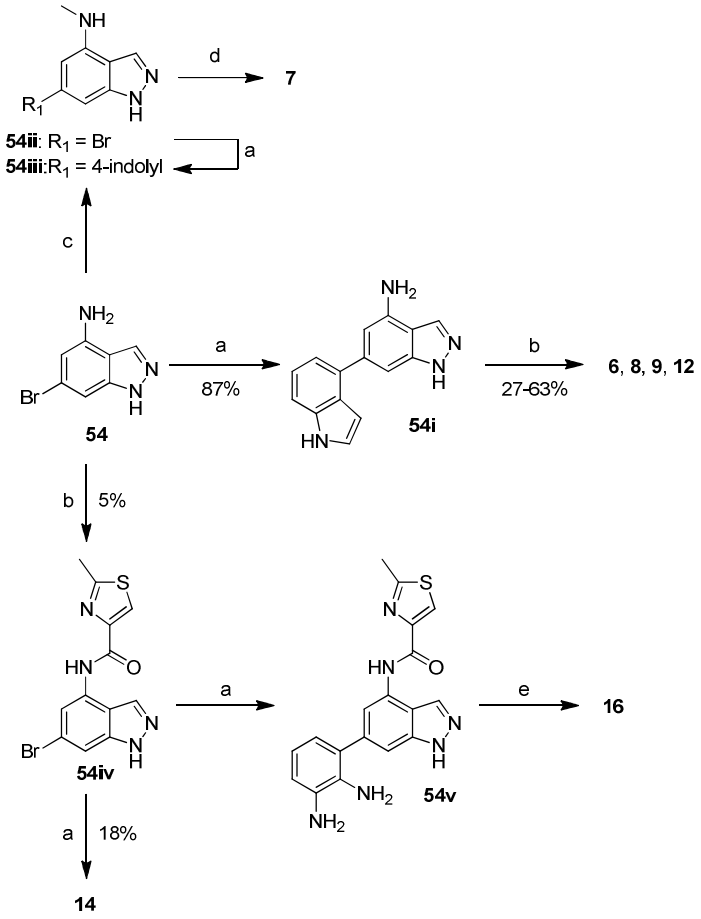


a) $Na_2CO_3$, $PdCl_2(dppf)$, 1,4-dioxane:water (1:1, v/v); b) HATU, DIPEA, DMF; c) paraformaldehyde, $NaBH_4$, NaOMe, MeOH; d) R-COCl, DIPEA, DCM; e) $HC(OEt)_3$, DMF.

Compounds prepared from compound **54vi** and **54xiii** are described in Scheme 3.

Reaction of compound **54** with benzenesulfonyl chloride gave compound **54vi** from which the intermediate **54vii** was generated using hexamethylditin and a palladium catalyst. A Stille coupling of compound **54vii** with the *N*-(5-bromo-3-pyridinyl)methanesulfonamide gave compound **54viii** which, after amide formation and deprotection, gave compound **49**.

In a further variant of this reaction scheme, compound **54vii** was transformed into compound **54ix** by amide coupling using HATU. A short sequence of Stille coupling with the appropriate bromide, followed by deprotection gave the compounds **17**, **18**, **50** and **43**.

A Suzuki-Miyaura cross-coupling reaction of intermediate **54vi** with indole-4-boronic acid gave compound **54x**. Amide formation with HATU and the appropriate carboxylic acid, followed by deprotection gave compounds **11** and **24**.

Amide formation using compound **54x** and 6-(chloromethyl)picolinoyl chloride gave compound **54xi** which was transformed into the amine **25** by treatment with piperidine, followed by deprotection. Similarly, compound **54x** could be transformed to compound **54xii** by reaction with 2-(chloromethyl)thiazole-4-carbonyl chloride after which amine displacement of the chloride followed by deprotection with potassium trimethylsilanolate gave compounds **27**, **28** and **29**.

Finally, tosyl protection of indazole **54** gave compound **54xiii** from which amide formation with 2-(chloromethyl)thiazole-4-carbonyl chloride gave intermediate **54xiv**. A short sequence of steps consisting of chloride displacement with (2*S*,6*R*)-2,6-dimethylmorpholine to give compound **54xv**, Suzuki coupling and subsequent deprotection gave compound **51**.

**Scheme 3.** Compounds prepared from compound **54vi** and **54xiii**.

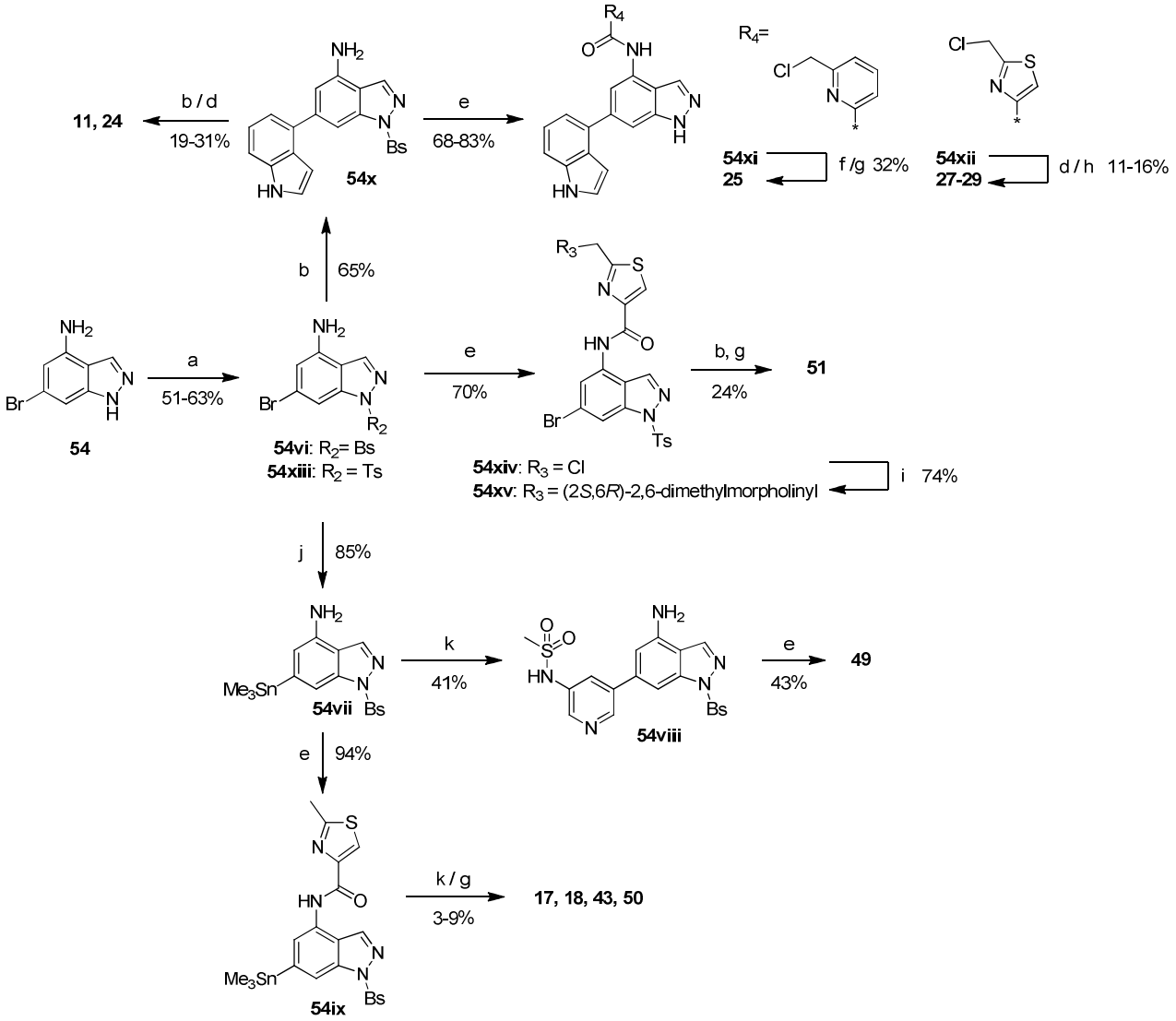


a) NaH, DMF, benzenesulfonyl chloride (54vi) or tosyl chloride (54xiii); b) $Na_2CO_3$, $PdCl_2$(dppf), 1,4-dioxane:water (1:1, v/v); c) HATU, DIPEA, DMF; d) Alkylamine, DIPEA, NaI, acetonitrile; e) R-COCl, DIPEA, DCM; f) Piperidine, acetonitrile; g) 2M NaOH (aq), IPA; h) $KOSi(CH_3)_3$, THF; i) (2*S*,6*R*)-2,6-Dimethylmorpholine; j) Hexamethylditin, triethylamine, $Pd(PPh_3)_4$; k) R-Br, $Pd(PPh_3)_4$ or chloro(di-2-norbornylphosphino)(2'-dimethylamino-1,1'-biphenyl-2-yl)palladium(II), DMF.

Compounds prepared from compound **55** are described in Scheme 4.

Protection of compound **55** with benzenesulfonyl chloride or tosyl chloride gave compounds **55i** and **55ii**, respectively. Suzuki-Miyaura cross-coupling of compound **55i** with 4-(4,4,5,5-tetramethyl-1,3,2-

dioxaborolan-2-yl)-1*H*-indole gave compound **55iii** which was converted to the tetrazole **55iv** using TMS-azide and dibutyl(oxo)stannane. Treatment of compound **55iv** with chloroacetyl chloride gave intermediate **55v** which was reacted with the appropriate amine and deprotected using sodium hydroxide to give compounds **40** and **41**.

Treatment of compound **55ii** with TMS-azide and dibutyl(oxo)stannane gave the intermediate **55vi** which was converted to oxadiazole **55vii** using acetyl chloride. Suzuki-Miyaura cross coupling with 4-(4,4,5,5-tetramethyl-1,3,2-dioxaborolan-2-yl)-1*H*-indole and concomitant deprotection gave compound **33**.

**Scheme 4.** Compounds prepared from compound **55**.

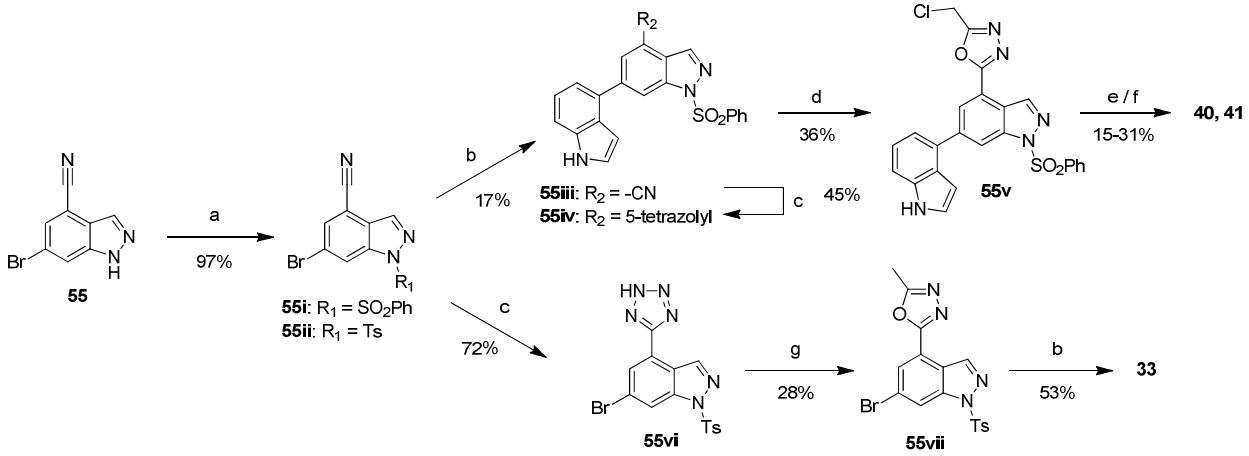


a) NaH, TsCl or $PhSO_2Cl$, DMF; b) $K_3PO_4$, $PdCl_2(dppf)$, 1,4-dioxane:water; c) dibutyl(oxo)stannane, TMS-$N_3$, toluene; d) Chloroacetyl chloride, $CHCl_3$; e) alkylamine, DIPEA, NaI, acetonitrile; f) 2M NaOH (aq), IPA; g) Acetyl chloride, toluene.

Compounds prepared from compound **56** are described in Scheme 5.

Protection of compound **56** with benzenesulfonyl chloride gave compound **56i** which could be converted to stannane **56ii** using hexamethylditin. Suzuki-Miyaura cross-coupling with TBDMS-

protected indole-4-boronic acid gave compound **56iii** which was transformed to compound **56iv** by Stille coupling with ethyl 2-chlorooxazole-4-carboxylate. Ester reduction with DIBAL-H gave alcohol **56v** which was converted to compound **56vi** with carbon tetrabromide and triphenylphosphine. Bromide displacement with the appropriate amine followed by deprotection with sodium hydroxide gave compounds **38** and **39**.

In a variant of this reaction scheme, Stille coupling of compound **56ii** with ethyl 2-chlorooxazole-5-carboxylate gave compound **56vii** which was reduced to compound **56viii** using DIBAL-H and converted to bromide **56ix** using carbon tetrabromide and triphenylphosphine with concomitant silyl deprotection. Reaction with the appropriate amine gave the intermediates **56x** and **56xi** and Suzuki-Miyaura cross-coupling with the appropriate aryl boronic acid or ester, followed by deprotection gave compounds **2**, **3** and **42**.

In a final variant of this scheme, compound **56i** was reacted with the appropriate oxazole zincate (formed by treatment of the 2-H oxazole with n-BuLi and $ZnCl_2$) to give intermediates **56xii** and **56xiii**. A Suzuki-Miyaura cross-coupling with 4-(4,4,5,5-tetramethyl-1,3,2-dioxaborolan-2-yl)-1*H*-indole, followed by sodium hydroxide deprotection gave compounds **31** and **32**.

**Scheme 5.** Compounds prepared from compound **56**.

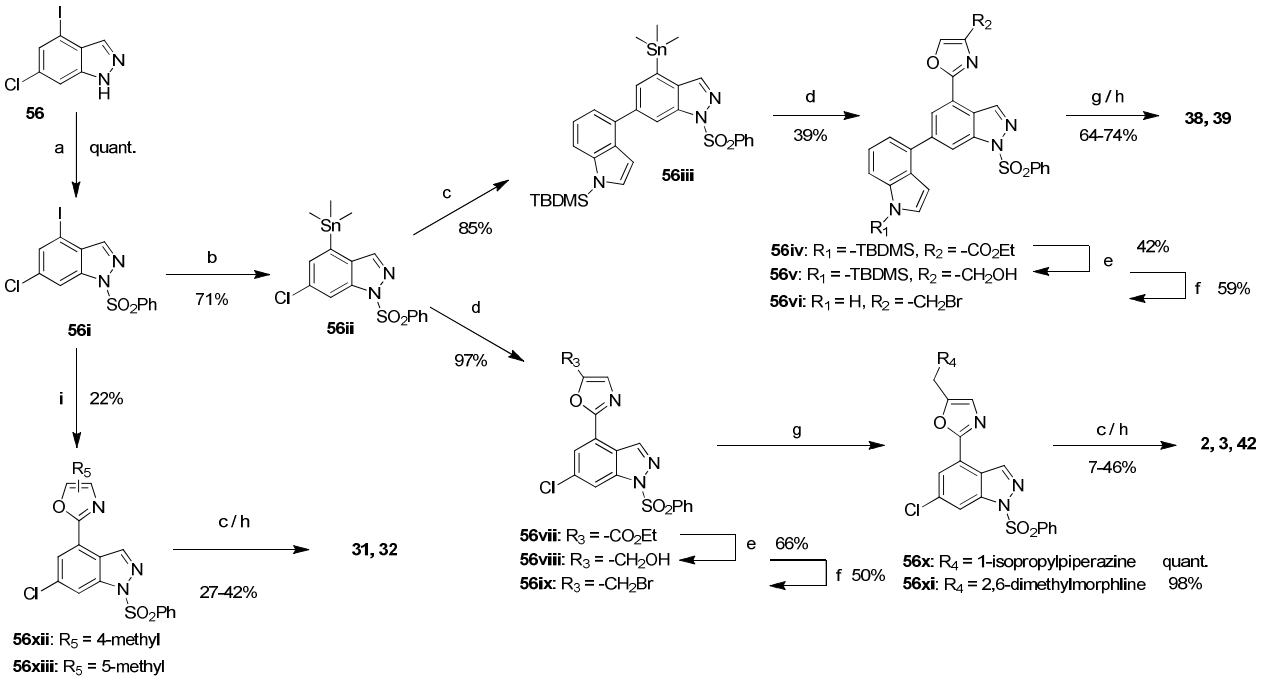


a) NaH, $PhSO_2Cl$, DMF; b) Hexamethylditin, triethylamine, $Pd(PPh_3)_4$; c) Chloro(di-2-norbornylphosphino)(2'-dimethylamino-1,1'-biphenyl-2-yl)palladium(II), $NaHCO_3$ or $K_3PO_4$, 1,4-dioxane:water; d) $Pd(PPh_3)_4$, CuI, DMF; e) 1M DIBAL-H, DCM; f) $CBr_4$, $PPh_3$, DCM; g) Alkylamine, DCM; h) 2M NaOH (aq), 1,4-dioxane; i) $ZnCl_2$, n-BuLi, $Pd(PPh_3)_4$, THF.

## Experimental Section

### Chemistry

General: All solvents and reagents, unless otherwise stated, were commercially available from regular suppliers such as Sigma-Aldrich and Fluorochem and were used as purchased without further purification. Proton and carbon nuclear magnetic resonance ($^1$H NMR and $^{13}$C NMR) spectra were recorded on a Bruker AVI (400 MHz), Bruker Nano (400 MHz) or Bruker AVII+ (600 MHz) spectrometer (with cryoprobe) in the indicated solvent. Chemical shifts δ are reported in parts per million (ppm) relative to tetramethylsilane and are internally referenced to the residual solvent peak. Coupling constants (J) are given in hertz (Hz) to the nearest 0.1 Hz. High resolution mass spectra (HRMS) were obtained on a Micromass Q-Tof Ultima hybrid quadrupole time-of-flight mass

spectrometer, equipped with a Z-spray interface (ESI), over a mass range of 100-1100Da, with a scan time of 0.9s and an interscan delay of 0.1s. Reserpine was used as the external mass calibrant ($[M+H]^+$ = 609.2812Da). The Q-Tof Ultima mass spectrometer was operated in W reflectron mode to give a resolution (FWHM) of 16000-20000. Ionisation was achieved with a spray voltage of 3.2kV, a cone voltage of 50V, with cone and desolvation gas flows of 10-20 and 600L/hr respectively. The source block and desolvation temperatures were maintained at 120ºC and 250ºC, respectively. The elemental composition was calculated using *MassLynx* v4.1 for the $[M+H]^+$ and the mass error quoted as ppm. LCMS methods are detailed in the supplementary information section. The purity of all compounds screened in the biological assays was examined by LCMS analysis and was found to be ≥95% unless otherwise specified.

6-Chloro-4-iodo-1-(phenylsulfonyl)-1*H*-indazole **56i**

To a stirring suspension of sodium hydride (60% dispersion on mineral oil) (35.5g, 889mmol) in DMF (200ml) at -15ºC was added a solution of 6-chloro-4-iodo-1*H*-indazole (198g, 711mmol) in DMF (600ml) dropwise. After complete addition the reaction mixture was stirred for 30min. Benzene sulfonyl chloride (100ml, 782mmol) was then added in DMF (200ml). Upon complete addition the reaction mixture was allowed to warm to room temperature and was left to stir overnight. The mixture was then poured onto ice/water (6L) with agitation. The resulting mixture was then filtered and the solid washed well with sodium bicarbonate (aq) and water. The solid was then dried *in vacuo* at 40ºC over the weekend to give title compound, 307g (quant.). $^1$H NMR (400 MHz, DMSO-$d_6$) $\delta_H$ 8.41 (d, *J*=0.8 Hz, 1H), 8.16 (s, 1H), 8.01 (dd, *J*=1.3, 8.5 Hz, 2H), 7.94 (d, *J*=1.5 Hz, 1H), 7.77 (t, *J*=7.5 Hz, 1H), 7.64 (t, *J*=7.8 Hz, 2H).

6-Chloro-1-(phenylsulfonyl)-4-(trimethylstannanyl)-1*H*-indazole **56ii**

A stirred solution of 6-chloro-4-iodo-1-(phenylsulfonyl)-1*H*-indazole (267g, 638mmol), hexamethylditin (253ml, 1218mmol), triethylamine (184ml, 1323mmol) and tetrakis(triphenylphosphine)palladium(0) (36.8g, 31.9mmol) in xylene (2.7L) was heated at 150ºC under nitrogen for 1.5h. The mixture was then filtered hot onto Celite® and washed with DCM. The filtrate was then evaporated and the residue solidified on standing. Cyclohexane (200ml) was added to the residue and it was heated to 60ºC in a water bath. Upon complete dissolution of the solid the solution was removed from the water bath. The solution was allowed to cool and crystallisation was initiated by scratching. The resulting suspension was diluted with cyclohexane and then filtered. The solid was washed sparingly with cyclohexane then dried *in vacuo* at 40ºC overnight to give title compound, 206g (71%). LCMS (method B) 83% product, rt 1.51min, $MH^+$ 457. $^1$H NMR (400 MHz, DMSO-$d_6$) $\delta_H$ 8.50 (d, *J*=0.5 Hz, 1H), 8.09 (dd, *J*=0.9, 1.6 Hz, 1H), 8.00 (dd, *J*=1.0, 8.5 Hz, 2H), 7.75 (t, *J*=7.5 Hz, 1H), 7.63 (t, *J*=7.8 Hz, 2H), 7.45 (d, *J*=1.8 Hz, 1H), 0.30-0.47 (m, 9H).

Ethyl 2-[6-chloro-1-(phenylsulfonyl)-1*H*-indazol-4-yl]-1,3-oxazole-5-carboxylate **56vii**

To a 3L rbf was added 6-chloro-1-(phenylsulfonyl)-4-(trimethylstannanyl)-1H-indazole (270g, 593mmol) and copper(I) iodide (11.29g, 59.3mmol). This was followed by a solution of ethyl 2-chloro-1,3-oxazole-5-carboxylate (135g, 771mmol) in dry degassed DMF (1L). To the mixture was added tetrakis(triphenylphosphine)palladium(0) (34.2g, 29.6mmol). The reaction mixture was further degassed by alternating nitrogen and vaccum to the vessel. The reaction was then heated to 100ºC and maintained at this temperature for 2h. The mixture was then filtered through Celite® and the pad washed with additional DMF (~350ml). The filtrate was then poured onto ice/water (8L) and the solid was then collected by filtration and dried *in vacuo* at 45ºC overnight. The solid was suspended in diethyl ether

(1.25L) and stirred for 30min. The suspension was then filtered and the solid was washed well with additional ether (1.25L). The solid was then dried *in vacuo* at 45ºC overnight to give title compound as a pale yellow solid, 249.47g (97%). LCMS (method B) 100% product, rt 1.37min $MH^+$ 432/434; $^1$H NMR (400 MHz, DMSO-$d_6$) $\delta_H$ 8.89 (d, *J*=1.0 Hz, 1H), 8.36-8.39 (m, 1H), 8.25 (s, 1H), 8.07 (s, 1H), 8.01 (d, *J*=1.8 Hz, 1H), 7.75-7.82 (m, 1H), 7.61-7.68 (m, 3H), 4.39 (q, *J*=7.2 Hz, 2H), 1.35 (t, *J*=7.2 Hz, 3H).

2-[6-Chloro-1-(phenylsulfonyl)-1*H*-indazol-4-yl]-1,3-oxazol-5-yl}methanol **56viii**

To solution of ethyl 2-[6-chloro-1-(phenylsulfonyl)-1*H*-indazol-4-yl]-1,3-oxazole-5-carboxylate (100g, 232mmol) in DCM (2L) maintained at -30ºC was added 1.5M DIBAL-H in toluene (400mL, 595mmol) dropwise via a peristaltic pump. The addition was controlled to stop addition when the temperature > -20ºC. Upon complete addition the reaction mixture was stirred at -30ºC for 3h. The mixture was quenched by the additon of methanol (200ml) maintaining the temperature below -20ºC. 2M HCl (aq.) (1L) was added and the layers were separated. Solid was observed in the aqueous phase and solid precipitated from the organic phase. The aqueous layer was extracted several times with 20% methanol in DCM. The combined organics were washed with brine. Solid began to precipitate so the brine was re-extracted with 20% methanol in DCM. The organics were combined and evaporated to a red-brown solid. The solid was then suspended in DCM (400ml) with stirring. Cyclohexane (200ml) was then added and stirring continued for a further 10 minutes. The suspension was then filtered and the solid was washed with cyclohexane:DCM (1:1). The solid was then dried *in vacuo* at 50ºC for 1h to give title compound, 59.16g (66%). LCMS (method B) 85% product, rt 1.09min $MH^+$ 390/392; $^1$H NMR (400 MHz, DMSO-$d_6$) $\delta_H$ 9.01 (d, *J*=0.8 Hz, 1H), 8.29 (dd, *J*=1.0, 1.5 Hz, 1H), 8.02-8.07 (m, 2H), 7.96 (d, *J*=1.5 Hz, 1H), 7.74-7.82 (m, 1H), 7.61-7.68 (m, 3H), 5.57 (t, *J*=5.8 Hz, 1H), 4.60 (d, *J*=5.3 Hz, 2H).

4-[5-(Bromomethyl)-1,3-oxazol-2-yl]-6-chloro-1-(phenylsulfonyl)-1*H*-indazole **56ix**

{2-[6-Chloro-1-(phenylsulfonyl)-1*H*-indazol-4-yl]-1,3-oxazol-5-yl}methanol (59.16g, 152mmol) and carbon tetrabromide (101g, 304mmol) in anhydrous DCM (1500ml) were cooled to -5ºC with stirring under a nitrogen atmosphere. Triphenylphosphine (80g, 304mmol) was added in portions keeping the temperature maintained between -5ºC and 0ºC. Upon complete addition the reaction mixture was allowed to warm to room temperature overnight. The reaction mixture was then partially concentrated *in vacuo* to ~200ml which was applied to a silica cartridge (1.5kg) that was eluted using a 0-40% ethyl acetate-DCM gradient. The appropriate fractions were combined and evaporated *in vacuo*. The solid was then re-dissolved in DCM (250ml) and applied to a silica cartridge (1.5kg) that was eluted using a 0-40% ethyl acetate-DCM gradient. The appropriate fractions were combined and evaporated *in vacuo* to give the desired product as a yellow solid, 34g (50%). LCMS (method B) 93% product, rt 1.42min $MH^+$ 452/454/456; $^1$H NMR (400 MHz, Chloroform-d) $\delta_H$ 8.93 (d, *J*=0.8 Hz, 1H), 8.38 (dd, *J*=1.0, 1.5 Hz, 1H), 8.05-8.07 (m, 1H), 8.04 (s, 1H), 8.01 (d, *J*=1.8 Hz, 1H), 7.61-7.66 (m, 1H), 7.49-7.55 (m, 2H), 7.29 (s, 1H), 4.60 (s, 2H).

6-Chloro-4-(5-{[4-(1-methylethyl)-1-piperazinyl]methyl}-1,3-oxazol-2-yl)-1-(phenylsulfonyl)-1*H*-indazole **56x**

1-Isopropylpiperazine (19.17ml, 134mmol) was added to a stirred solution of 4-[5-(bromomethyl)-1,3-oxazol-2-yl]-6-chloro-1-(phenylsulfonyl)-1*H*-indazole (28.6g, 63.2mmol) in DCM) (300ml) and the reaction mixture was stirred at room temperature for 2h. Water was added and the mixture stirred well. The layers were separated and the aqueous extracted with additional DCM. The combined organics were then washed with brine, dried over magnesium sulfate then filtered and evaporated to give title compound as a yellow solid, 32.57g (quant.) used without further purification. LCMS (method B) 97%

product, rt 0.96min $MH^+$ 500/502; $^1H$ NMR (400 MHz, Chloroform-d) $\delta_H$ 8.93 (d, *J*=0.8 Hz, 1H), 8.33 (dd, *J*=0.9, 1.6 Hz, 1H), 8.00-8.09 (m, 2H), 7.98 (d, *J*=1.8 Hz, 1H), 7.59-7.66 (m, 1H), 7.48-7.56 (m, 2H), 7.15 (s, 1H), 3.73 (s, 2H), 2.50-2.73 (m, 8H), 1.64-1.78 (m, 1H), 1.06 (d, *J*=6.3 Hz, 6H).

6-(1*H*-Indol-4-yl)-4-(5-{[4-(1-methylethyl)-1-piperazinyl]methyl}-1,3-oxazol-2-yl)-1*H*-indazole **2 (GSK2269557)**

6-Chloro-4-(5-{[4-(1-methylethyl)-1-piperazinyl]methyl}-1,3-oxazol-2-yl)-1-(phenylsulfonyl)-1*H*-indazole (5g, 10mmol), 4-(4,4,5,5-tetramethyl-1,3,2-dioxaborolan-2-yl)-1H-indole (4.86g, 20mmol), sodium bicarbonate (2.52 g, 30mmol) and chloro(di-2-norbornylphosphino)(2'-dimethylamino-1,1'-biphenyl-2-yl)palladium(II) (0.56g, 1mmol) were charged to a 250ml round bottomed flask. 1,4-Dioxane (80ml) and water (20ml) were charged and the reaction vessel heated to 120ºC. The temperature was maintained for 2.5hrs. The reaction mixture was then cooled to room temperature and was then treated with sodium hydroxide (aq. 2M) (35ml, 70mmol) and stirring continued at room temperature. The reaction mixture was then left stirring at room temperature overnight. DCM (200ml) and water was added then the mixture filtered through celite. The filtrate was then re-filtered through celite and the filtrate was then separated and the aqueous was re-extracted with DCM:1,4-dioxane (2:1, 100ml). The combined organics were then extracted with 2M HCl (aq.) (1x150ml). The extractions were filtered through Celite®. The organic was re-extracted a further 2 times using 2M HCl (aq.) (2x150ml), filtering each extraction through Celite®. The combined acidic aqueous phase was further filtered through Celite® then basified using 10M NaOH (aq) to pH 14. 20% methanol in DCM was added and the compund was extracted a number of times to dissolve all the compound. The combined organics were combined and evaporated and the residue was dissolved in DMF/TFA (2:1, 15ml) then applied to a $C_{18}$ reverse phase column (330g) washing on with DMF/TFA (1:1, 5ml). The column was then eluted

with 3-40% acetonitrile in water containing 0.25% TFA. Fractions were combined and the acetonitrile was removed *in vacuo*. The acidic aqueous was then basified using saturated sodium carbonate (aq) (~100ml). The solid precipitate was then collected by filtration and washed well with water. The solid was then dried *in vacuo* at 50ºC over the weekend to give title compound as a white solid, 2.02g (46%). LCMS (method B) 100% product, rt 0.67min $MH^+$ 441; $^1$H NMR (400 MHz, DMSO-$d_6$) $\delta_H$ 13.40 (br. s., 1H), 11.34 (br. s, 1H), 8.60 (s, 1H), 8.08 (d, *J*=1.5 Hz, 1H), 7.88-7.94 (m, 1H), 7.44-7.52 (m, 2H), 7.32 (s, 1H), 7.21-7.29 (m, 2H), 6.58-6.63 (m, 1H), 3.74 (s, 2H), 2.61 (br. s, 1H), 2.33-2.58 (m, 8H), 0.95 (d, *J*=6.6 Hz, 6H). $^{13}$C NMR (126 MHz, DMSO-$d_6$) $\delta_C$ 160.5, 149.9, 141.6, 139.5, 136.9, 134.1, 132.8, 127.8, 126.7, 126.2, 122.0, 120.4, 119.6, 119.5, 118.5, 111.8, 100.4, 54.1, 52.9, 51.9, 48.4, 18.6; HRMS (ESI): m/z ($MH^+$) 441.2396. Calc. = 441.2403.

6-Chloro-4-(5-{[(2*R*,6*S*)-2,6-dimethyl-4-morpholinyl]methyl}-1,3-oxazol-2-yl)-1-(phenylsulfonyl)-1*H*-indazole **56xi**

4-[5-(Bromomethyl)-1,3-oxazol-2-yl]-6-chloro-1-(phenylsulfonyl)-1*H*-indazole (4.9g, 10.82mmol) was dissolved in anhydrous DCM (75ml), (2*R*,6*S*)-2,6-dimethylmorpholine (2.76ml, 21.65mmol) was added and the reaction mixture stirred at room temperature for 1.5h. The reaction mixture was extracted twice with water (50ml). The DCM layer was passed through a hydrophobic frit and evaporated to dryness under reduced pressure. The resulting yellow solid was placed in a vacuum oven at 50ºC overnight to give title compound, 5.16g (98%), used without further purification. LCMS (method B) 94% product, rt 1.01min $MH^+$ 487/489; $^1$H NMR (400 MHz, Chloroform-d) δ 8.94 (d, *J*=0.5 Hz, 1H), 8.32-8.36 (m, 1H), 8.04-8.06 (m, 1H), 8.03 (d, *J*=1.5 Hz, 1H), 7.99 (d, *J*=1.8 Hz, 1H), 7.60-7.65 (m, 1H), 7.49-7.55 (m, 2H), 7.16 (s, 1H), 3.69-3.76 (m, 2H), 3.68 (s, 2H), 2.77 (d, *J*=10.3 Hz, 2H), 1.87 (dd, *J*=10.1, 11.3 Hz, 2H), 1.17 (d, *J*=6.3 Hz, 6H).

*N*-[5-[4-(5-{[(2*R*,6*S*)-2,6-Dimethyl-4-morpholinyl]methyl}-1,3-oxazol-2-yl)-1*H*-indazol-6-yl]-2-(methyloxy)-3- pyridinyl]methanesulfonamide **3 (GSK2292767)**

*N*-[2-(Methyloxy)-5-(4,4,5,5-tetramethyl-1,3,2-dioxaborolan-2-yl)-3-pyridinyl]methanesulfonamide (1.7g, 5.18mmol), 6-chloro-4-(5-{[(2*R*,6*S*)-2,6-dimethyl-4-morpholinyl]methyl}-1,3-oxazol-2-yl)-1-(phenylsulfonyl)-1*H*-indazole (2.8g, 5.18mmol) and sodium bicarbonate (1.31g, 15.54mmol) were suspended in 1,4-dioxane (10ml) and water (20ml) under a nitrogen atmosphere and heated to 80ºC. Chloro(di-2-norbornylphosphino)(2'-dimethylamino-1,1'-biphenyl-2-yl)palladium(II) (0.29g, 0.518mmol) was added and the mixture was stirred overnight at 80ºC. The reaction mixture was cooled to 45ºC and sodium hydroxide (2M aq.) (12.95ml, 25.9mmol) was added and heating continued for 4h. The reaction mixture was then cooled to room temperature and neutralised using 2M hydrochloric acid (12.95ml, 25.9mmol). The reaction mixture was then extracted with DCM (4x50ml) and the combined organic layers were dried over magnesium sulfate and concentrated *in vacuo*. The mixture was purified via a 120g silica column system using isocratic toluene/ethanol/ammonia (78:20:2). The pure fractions were combined, evaporated and then recrystallised with ethanol (2.8ml). The resulting suspension was filtered and the solid washed with ethanol and dried in a vacuum oven, to give title compound, 194mg (7%). LCMS (method B) 100% product, rt 0.6min $MH^+$ 513; $^1$H NMR (400 MHz, DMSO-$d_6$) $\delta_H$ 13.5 (br. s, 1H), 9.39 (s, 1H), 8.58 (s, 1H), 8.42 (d, *J*=2.5 Hz, 1H), 8.00 (d, *J*=2.3 Hz, 1H), 7.94 (d, *J*=1.5 Hz, 1H), 7.88 (s, 1H), 7.36 (s, 1H), 4.01 (s, 3H), 3.74 (s, 2H), 3.54-3.63 (m, 2H), 3.12 (s, 3H), 2.81 (d, *J*=9.9 Hz, 1H), 1.78 (t, *J*=10.6 Hz, 1H), 1.05 (d, *J*=6.3 Hz, 6H); $^{13}$C NMR (101 MHz, DMSO-$d_6$) $\delta_C$ 160.3, 156.8, 149.7, 141.6, 141.4, 135.4, 134.1, 131.3, 130.0, 128.0, 121.9, 120.1, 118.9, 118.4, 110.6, 71.4, 58.8, 54.3, 51.8, 41.2, 19.4; HRMS (ESI): m/z ($MH^+$) 513.1929. Calc. = 513.1920.

## Biology

### PI3Kα, β, γ, and δ HTRF Assays

#### Standard HTRF assay

Inhibition of PI3Kinase enzymatic activity was determined using a homogeneous time resolved fluorescence (HTRF) kit assay format provided by Millipore. Reactions were performed in assay buffer containing 50 mM HEPES, pH 7.0, 150 mM NaCl, 10 mM $MgCl_2$, < 1 % cholate (w/v), < 1 % CHAPS (w/v), 0.05 % sodium azide (w/v) and 1 mM DTT. Enzymes were preincubated with compound, serially diluted 4-fold in 100 % DMSO, for 15 mins prior to reaction initiation upon addition of substrate solution containing ATP at $K_m$ for the specific isoform tested (α at 250 μM, β at 400 μM, δ at 80 μM and γ at 15 μM), PIP2 at either 5 μM (PI3Kδ) or 8 μM (PI3Kα, β and γ) and 10nM biotin-PIP3. Assays were quenched after 60 mins by addition of a quench/detection solution prepared in 50 mM HEPES pH 7.0, 150 mM NaCl, < 1 % cholate, < 1 % Tween 20, 30 mM EDTA, 40 mM potassium fluoride and 1 mM DTT containing 16.5 nM GRP-1 PH domain, 8.3 nM Streptavidin-APC and 2 nM Europium-anti-GST, and were left for a further 60 mins in the dark to equilibrate prior to reading using a BMG RubyStar plate reader. Ratio data were normalised to high (no compound) and low (no enzyme) controls prior to fitting using a logistical four parameter equation to determine $IC_{50}$.

#### Modified HTRF assay

Inhibition of PI3Kinase enzymatic activity was determined using a homogeneous time resolved fluorescence (HTRF) assay format. Reactions were performed in assay buffer containing 50 mM HEPES, pH 7.0, 150 mM NaCl, 10 mM $MgCl_2$, 2.3 mM sodium cholate, 10 μM CHAPS and 1 mM DTT. Enzymes were preincubated with compound, serially diluted 4-fold in 100% DMSO, for 20min

prior to reaction initiation upon addition of substrate solution containing ATP, at either $K_m$ for the specific isoform tested (α at 250μM, β at 400μM, δ at 80μM and γ at 15μM) or at 2mM, approx. 10μM PIP2 and 10nM biotin-PIP3. Assays were quenched after 60min by addition of a quench/detection solution prepared in 50mM HEPES pH 7.0, 150mM NaCl, 2.3mM sodium cholate, 10μM CHAPS, 30mM EDTA, 40mM potassium fluoride and 1mM DTT containing 16.5nM GRP-1 PH domain, 8.3nM Streptavidin-APC and 2nM Europium-anti-GST, and were left for a further 60min in the dark to equilibrate prior to reading using a PerkinElmer Envision plate reader. Ratio data were normalised to high (no compound) and low (either enzyme in the presence of 8.3μM wortmannin or no enzyme) controls prior to fitting using a logistical four parameter equation to determine $IC_{50}$.

**Peripheral blood mononuclear (PBMC) assay**

Reagents were purchased from Invitrogen Corporation Ltd. Unless specified. PBMC cells (peripheral blood mononuclear cells) were prepared from heparinised human blood (using 1% v/v Heparin Sodium 1000 U/ml Endotoxin Free, Leo Laboratories Ltd.) using the Accuspin™ System-Histopaque™-1077 (Sigma-Aldrich Company Ltd.). The cells were resuspended in RPMI1640 medium containing 10% foetal calf serum, 1% L-glutamine and 1% penicillin/streptomycin. The cells at a density of 5x105 viable cells/ml were incubated with 0.0156% (v/v) CytoStim (Miltenyi Biotech). The assay plate was then incubated at 37ºC, 5% $CO_2$, for 20 hours. The supernatant was removed and the concentrations of IFNγ was determined by electrochemiluminescence assay using the Meso Scale Discovery (MSD) technology (Meso Scale Discovery).

**Brown Norway Rat acute OVA model of Th2 driven lung inflammation**

All reagents unless stated were from Sigma Aldrich. The models used in these studies conform to UK standards of animal care, as laid down by the Home Office. Procedures were carried out as exactly specified under GlaxoSmithKline's Respiratory Diseases Project licence (PPL – 80/2361 and 80/1537). Male Brown Norway (BN) rats, weighing 250 to 300g were sensitised by intraperitoneal injection of a 1ml OVA solution containing 10μg of OVA and 20mg of $Al(OH)_3$ on day 1 and 7. On day 21 or 28 rats were challenged with 0.2ml intra-tracheal OVA solution under isoflurane (Abbott Laboratories) anaesthesia. Compound in vehicle (0.2% Tween 80 water pH 4.5) or vehicle alone was also dosed by i.t. route (0.2ml volume) at t-30 minutes and +24 hours relative to intra-tracheal OVA challenge. 48 hours after i.t. OVA challenge rats were sacrificed by anaesthetic overdose. The trachea was exposed and lungs lavaged with 5ml lavage fluid (0.1% BSA, 10mM EDTA and 1 protease inhibitor tablet Cat 11873580001 from Roche per 50ml). Death was confirmed by cervical dislocation. BAL was immediately transferred onto ice and leucocytes were then quantified by flow cytometry. Briefly, samples were read on a BD FACSCANTO II 8 colour flow cytometer. Lymphocytes, Eosinophils, neutrophils and macrophages were gated on FSC and SSC using morphological criteria. Threshold was set on FSC channel. In some studies the Amcyan channel was used to gate cells further using autofluorescence (intersecting gates). DAPI+ cells were excluded as dead. For cytokine analysis mice were lavaged 24 hours after Ova challenge. BAL was spun at 4ºC at 300g for 7 min and the supernatant stored at 20ºC prior to analysis. Data from repeat studies were average-standardised, pooled and a 4-parameter non-linear logistic curve fitted.

**Human lung parenchyma assay**

Human lung fragments were prepared as previously described[30] from three donors by removing the large airways and the outer layer of the parenchyma and by fine slicing in assay buffer containing;

RPMI-1640 supplemented with 100units/ml Penicillin, 100µg/ml Streptomycin (all from Gibco, UK), 2mM L-glutamine, and 0.1% BSA (both from Invitrogen, UK). The preparations were then filtered through a 1mm sieve. The filtered lung parenchyma fragments were incubated with compound or DMSO for 1h, and then incubated with 10µg/ml phytohaemagglutanin (PHA; Sigma, UK). 72 hours later, levels of IFNγ and IL2 were measured in the culture supernatants following the manufacturer's protocol for the corresponding multiplex immunoassay plate (Meso Scale Discovery, Gaithersburg, MD, USA). The electro chemo-luminescent values were normalised to percentage inhibition (%I) relative to the unstimulated lung parenchyma fragment mean values and to the stimulated DMSO control mean values. $IC_{50}$ values were estimated by fitting %I obtained for each donor to the four-parameter logistic equation $\%I = \{(Max - Min)/[1 + ([I]/IC_{50})h] + Min$, where Max is the estimated maximum inhibition, Min the estimated minimum inhibition, [I] is the inhibitor concentration and h is the Hill slope.

**hERG FP assay**

Inhibition of hERG enzymatic activity was determined using a fluorescence polarisation (FP) assay format. Reactions were performed in assay buffer containing 25mM HEPES, pH 7.4, 100mM KCl and 1.2mM $MgCl_2$. The hERG membranes (from CHO cells) were diluted to approx. 0.06mg/mL in buffer containing the Cy3b-labelled dofelitide ligand at 1nM and 0.1 % (v/v) Pluronic acid (F127) and left to equilibrate for 75min at room temperature. The membrane/ligand solution was subsequently preincubated with compound, serially diluted in 100 % DMSO, for 75min prior to reading using an LJL Acquest plate reader. Ratio data were normalised to high (no compound) and low (10µM Astemizole) controls prior to fitting using a logistical four parameter equation to determine $IC_{50}$.

**Rabbit wedge assay**

The rabbit ventricular wedge assay has been described previously[31]. Briefly, a transmural wedge was dissected from the left ventricle of female rabbit hearts (New Zealand White rabbits; 2.0-3.0 kg; sedated with xylazine (6mg/kg, s.c.), anticoagulated with heparin, and anaesthetised with pentobarbital (50mg/kg, i.v.)) following cannulation and perfusion of the left circumflex/descending branch of the coronary artery with cold cardioplegic solution (24mM potassium ($K^+$), buffered with 95% $O_2$/5% $CO_2$). The preparation was then placed in a tissue bathand arterially perfused with Tyrode's solution (4mM K+, buffered with 95% $O_2$/5% $CO_2$, approximately 35.7ºC). The preparation was paced at 1 and 0.5 hertz (Hz) (equivalent to 60 and 30 beats per minute (bpm), respectively) using a bipolar silver electrode applied to the endocardial surface, and was exposed to each test concentration for approximately 30 minutes. A transmural ventricular electrocardiogram (ECG) was recorded from each preparation at the different stimulation frequencies. The parameters measured were QT interval, Tpeak-end (Tp-e), and QRS interval.

**Pharmacokinetic studies**

*In vitro* clearance was determined to assess metabolic stability of compounds in rat microsomes. Microsomes (190µL, 0.5mg protein/mL) were pre-warmed for 10mins at 37°C. The incubation was initiated by addition of NADPH regeneration system (50µL) and compound (10µL, 12.5uM) resulting in a final compound concentration of 0.5µM in the incubation. Samples (20µL) were removed at 0, 3, 6, 12 and 30 minutes and the reaction quenched by addition to acetonitrile (100µL) containing internal standard (IS). Compound remaining was measured using specific LC-MS/MS methods as a ratio to the internal standard in the absence of a calibration curve. Peak area ratios (Compound to IS) were fitted to an unweighted logarithmic decline in substrate. Using the first order rate constant, clearance was

calculated by adjustment for protein concentration (0.5mg/mL), volume of the incubation (250µL) and hepatic scaling factor (52.5mg microsomal protein/g liver).

*In vivo* pharmacokinetics was tested in Sprague Dawley male rats. Compounds were administered discretely by the oral or intravenous routes, at a dose level of 3 and 1mg/kg respectively (n=2 rats/route). Compounds were formulated as a solution in DMSO:PEG200:water (5:45:50 v/v/v) at a dose volume of 6 (oral) and 2 (intravenous) ml/kg. All animals were serially bled from the tail vein and blood samples collected over a time-course of 0-7h were submitted to LC-MS/MS analysis for the quantification of the parent compound. The main pharmacokinetic parameters were estimated by non-compartmental analysis.

**Physicochemical studies**

**pKa determination.** The pKa was measured using Sirius T3 Fast UV pKa method. The sample was run under the spectrophotometric (UV-metric) method on a Sirius T3 instrument covering the pH range 2-12. 5µl of 10 mM DMSO stock solution was used in the co-solvent method utilising MeOH as co-solvent. Data were refined using the Yasuda-Shedlovsky extrapolation.

**Chemi-Luminescent Nitrogen Detection (CLND) Solubility Determination.**

GSK in-house kinetic solubility assay: 5ml of 10mM DMSO stock solution diluted to 100µL with pH 7.4 phosphate buffered saline, equilibrated for 1h at room temperature, filtered through Millipore MultiscreenHTS-PCF filter plates (MSSL BPC). The filtrate was quantified by suitably calibrated flow injection chemiluminescent nitrogen detection.[16] The standard error of the CLND solubility determination was ±30 µM, and the upper limit of the solubility is 500µM when working from 10mM DMSO stock solution.

All animal studies were ethically reviewed and carried out in accordance with Animals (Scientific Procedures) Act 1986 and the GSK Policy on the Care, Welfare and Treatment of Laboratory Animals. The human biological samples were sourced ethically and their research use was in accord with the terms of the informed consents.

## ASSOCIATED CONTENT

### Supporting Information

Complete experimental for all other intermediates and final compounds; X-ray crystallography table of statistics and density maps for compounds **2** and **3**; kinase profiling data for compounds **2**, **3**, **28** and **29**. PDB codes to be added once the manuscript is accepted for publication. This material is available free of charge via the Internet at http://pubs.acs.org.

## AUTHOR INFORMATION

### Corresponding Author

Nicole Hamblin: email: nicole.j.hamblin@gsk.com; telephone: 00441438763349.

## ACKNOWLEDGEMENTS

The authors would like to thank Ian Reid for p$K_a$ data generation; Paul Carter, Phil Hardwicke, Julie Mosley and Maire Convery for protein production, purification and crystallography assistance; Linda Warnock and Mark Lennon for the statistical evaulation of the OVA data and generation of $ED_{50}$ values for compounds **2** and **3**; Sara Graham for the rabbit wedge data; Ramulu Akula, Aurelie Champigny, Karl Collins, Paul Cox, Xavier Just Baringo, Vaishali Gupta, Mark Howard, Jordi Juarez-Jimenez,

Camille Mesnage, Arunoday Singh, Fabien Schaeffer and Natalie Wellaway for their synthetic contributions; and David House for review of the manuscript.

**ABBREVIATIONS USED**

DIPEA, diisopropylethylamine; HAC, heavy atom count; HATU, (1-[bis(dimethylamino)methylene]-1H-1,2,3-triazolo[4,5-b]pyridinium 3-oxid hexafluorophosphate); HTRF, homogeneous time resolved fluorescence; IFNγ, interferon gamma; IL, interluekin; OVA, ovalbumin; PBMC, peripheral blood mononuclear cell; PHA, lectin phytohaemagglutanin; TBDMS, tert-butyldimethylsilyl; TdP, Torsades de Pointes; Th2, Type 2 helper T-cells.

**References**

(1) Cantley, L. C. The phosphoinositide 3-kinase pathway. *Science* **2002**, *296*, 1655-1657.

(2) Vanhaesebroeck, B.; Guillermet-Guibert, J.; Graupera, M.; Bilanges, B. The emerging mechanisms of isoform-specific PI3K signalling. *Nat. Rev. Mol. Cell Biol.* **2010**, *11*, 329-341.

(3) Foster, J. G.; Blunt, M. D.; Carter, E.; Ward, S. G. Inhibition of PI3K signaling spurs new therapeutic opportunities in inflammatory/autoimmune diseases and hematological malignancies. *Pharm Rev.* **2012**, *64*, 1027-1054.

(4) Engelman, J. A.; Luo, J.; Cantley, L. C. The evolution of phosphatidylinositol 3-kinases as regulators of growth and metabolism. *Nat. Rev. Genet.* **2006**, *7*, 606-619.

(5) McNamara, C. R.; Degterev, A. Small-molecule inhibitors of the PI3K signaling network. *Future Med. Chem.* **2011**, *3*, 549-565.

(6) Rowan, W. C.; Smith, J. L.; Affleck, K.; Amour, A. Targeting phosphoinositide 3-kinase δ for allergic asthma. *Biochem. Soc. Trans.* **2012**, *40*, 240–245

(7) Sriskantharajah S.; Hamblin N.; Worsley S.; Calver A. R.; Hessel E. M.; Amour A. Targeting phosphoinositide 3-kinase δ for the treatment of respiratory diseases. *Ann. N. Y. Acad. Sci.* **2013**, *1280*, 35-39.

(8) Ball, J.; Archer, S.; Ward, S. PI3K inhibitors as potential therapeutics for autoimmune disease. *Drug Discovery Today* **2014**, *19*, 1195-1199.

(9) Vanhaesebroeck, B.; Ali, K.; Bilancio, A.; Geering, B.; Foukas, L. C. Signalling by PI3K isoforms: insights from gene-targeted mice. *Trends Biochem. Sci.* **2005**, *30*, 194−204.

(10) Rückle, T.; Schwarz, M. K.; Rommel, C. PI3Kγ inhibition: towards an 'aspirin of the 21st century'? *Nat. Rev. Drug Discov.* **2006**, *5*, 903−918.

(11) Dienstmann, R.; Rodon, J.; Serra, V.; Tabernero, J. Picking the point of inhibition: A comparative review of PI3K/AKT/mTOR pathway inhibitors. *Mol. Cancer Ther.* **2014**, *13*, 1-11.

(12) Bamborough, P.; Christopher, J. A.; Cutler, G. J.; Dickson, M. C.; Mellor, G. W.; Patel, C. B.; Shewchuk, L. M. 5-(1H-Benzimidazol-1-yl)-3-alkoxy-2-thiophenecarbonitriles as potent, selective, inhibitors of IKK-ε kinase. *Bioorg. Med. Chem. Lett.* **2006**, *16*, 6236-6240.

(13) PI3Kinases catalyse the $Mg2^{+}$-ATP-dependent generation of PIP3 from PIP2, which competes directly with a biotinylated PIP3 tracer for binding to a recombinant GRP-1 PH-domain in the formation of an energy transfer complex.

(14) Borgström, L.; Olsson, B.; Thorsson, L. Degree of throat deposition can explain the variability in lung deposition of inhaled drugs. *J. Aerosol Med.* **2006**, *19*, 473-483

(15) A homology model of PI3Kδ was developed using an X-ray structure of PI3Kγ (1vgwt) as a template and using the Biopolymer Composer module in Sybyl v7.2.

(16) Bhattachar, S. N.; Wesley, J. A.; Seadeek, C. Evaluation of the chemiluminescent nitrogen detector for solubility determinations to support drug discovery. *J. Pharm. Biomed. Anal.* **2006**, *41*, 152−157.

(17) ClogP by Biobyte Version 4.0 (http://www.biobyte.com/index.html)

(18) Sutherlin, D. P.; Baker, S.; Bisconte, A.; Blaney, P. M.; Brown, A.; Chan, B. K.; Chantry, D.; Castenedo, G.; DePledge, P.; Goldsmith, P.; Goldstein, D. M.; Hancox, T.; Kaur, J.; Knowles, D.; Kondru, R.; Lesnick, J.; Lucas, M. C.; Lewis, C.; Murray, J.; Nadin, A. J.; Nonomiya, J.; Pang, J.; Pegg, N.; Price, S.; Reif, K.; Safina, B. S.; Salphati, L.; Staben, S.; Seward, E. M.; Shuttleworth, S.; Sohal, S.; Sweeney, Z. K.; Ultsch, M.; Waszkowycz, B.; Wei, B. Potent and selective inhibitors of PI3Kδ: Obtaining isoform selectivity from the affinity pocket and tryptophan shelf. *Bioorg. Med. Chem. Lett.* **2012**, *22*, 4296-4302.

(19) In-house kinase panel consisting of protein kinases such as IKK2, ALK5, JNK3 etc. Full data is provided in the supporting information.

(20) Laurence, C.; Brameld, K. A.; Graton, J.; Le Questel, J.-Y.; Renault, E. The p$K_{BHX}$ database: Toward a better understanding of hydrogen-bond basicity for medicinal chemists. *J. Med. Chem.* **2009**, *52*, 4073-4086.

(21) Peterson, L.A. Reactive metabolites in the biotransformation of molecules containing a furan ring. *Chem. Res. Toxicol.* **2013**, *26*, 6-25.

(22) Gribble, F. M.; Loussouarn, G.; Tucker, S. J.; Zhao, C.; Nichols, C. G.; Ashcroft, F. M. A novel method for measurement of submembrane ATP concentration. *J. Biol. Chem.* **2000**, *275*, 30046-30049.

(23) http://www.merckmillipore.com

(24) Stocks, M. J.; Alcaraz, L.; Bailey, A.; Bonnert, R.; Cadogan, E.; Christie, J.; Dixon, J.; Connolly, S.; Cook, A.; Fisher, A.; Flaherty, A.; Humphries, A.; Ingall, A.; Jordan, S.; Lawson, M.; Mullen, A.; Nicholls, D.; Paine, S.; Pairaudeau, G.; Young, A. Discovery of AZD3199, an inhaled ultralong acting $\beta_2$ receptor agonist with rapid onset of action. *ACS Med. Chem. Lett.* **2014**, *5*, 416-421.

(25) A dose of 1mg per day is the notional maximum amount of API that can reasonably be delivered by current inhaler technology.

(26) Aronov, A. M. Common pharmacophores for uncharged human ether-a-go-go-related gene (hERG) blockers. *J. Med. Chem.* **2006**, *49*, 6917-6921.

(27) Knight, S. D.; Adams, N. D.; Burgess, J. L.; Chaudhari, A. M.; Darcy, M. G.; Donatelli, C. A.; Leungo, J. I.; Newlander, K. A.; Parrish, C. A.; Ridgers, L. H.; Sarpong, M. A.; Schmidt, S. J.; Van Aller, G. S.; Carson, J. D.; Diamond, M. A.; Elkins, P. A.; Gardiner, C. M.; Garver, E.; Gilbert, S. A.; Gontarek, R. R.; Jackson, J. R.; Kershner, K. L.; Luo, L.; Raha, K.; Sherk, C. S.; Sung, C.-M.; Sutton, D.; Tummino, P. J.; Wegrzyn, R. J.; Auger, K. R.; Dhanak, D. Discovery of GSK2126458, a highly potent inhibitor of PI3K and the mammalian target of rapamycin. *ACS Med. Chem. Lett.* **2010**, *1*, 39-43.

(28) Berndt, A.; Miller, S.; Williams, O.; Le, D. D.; Houseman, B. T.; Pacold, J. I.; Gorrec, F.; Hon, W.-C.; Ren, P.; Liu, Y.; Rommel, C.; Gaillard, P.; Rückle, T.; Schwarz, M. K.; Shokat, K. M.; Shaw, J. P.; Williams, R. L. The p110δ structure: mechanisms for selectivity and potency of new PI(3)K inhibitors. *Nat. Chem. Biol.* **2010**, *6*, 117-124.

(29) Hopkins, A. L.; Groom, C. R.; Alex, A. Ligand efficiency: a useful metric for lead selection. *Drug Discovery Today.* **2004**, *9*, 430-431.

(30) Rice, L.V; Bax, H.J.; Russell, L. J.; Barrett, V. J.; Walton, S. E.; Deakin, A.M.; Thomson, S.A.; Lucas, F.; Solari, R.; House D.; Begg, M. Characterization of selective calcium-release activated calcium channel blockers in mast cells and T-cells from human, rat, mouse and guinea-pig preparations. *Eur. J. Pharm.* **2013**, *704*, 49-57.

(31) 10. T. Liu, B. S. Brown, Y. Wu, C. Antzelevitch, P. R. Kowey, G. X. Yan, Blinded validation of the isolated arterially perfused rabbit ventricular wedge in preclinical assessment of drug-induced proarrhythmias. *Heart Rhythm* **2006**, *3*, 948-956.

Table of Contents Graphic

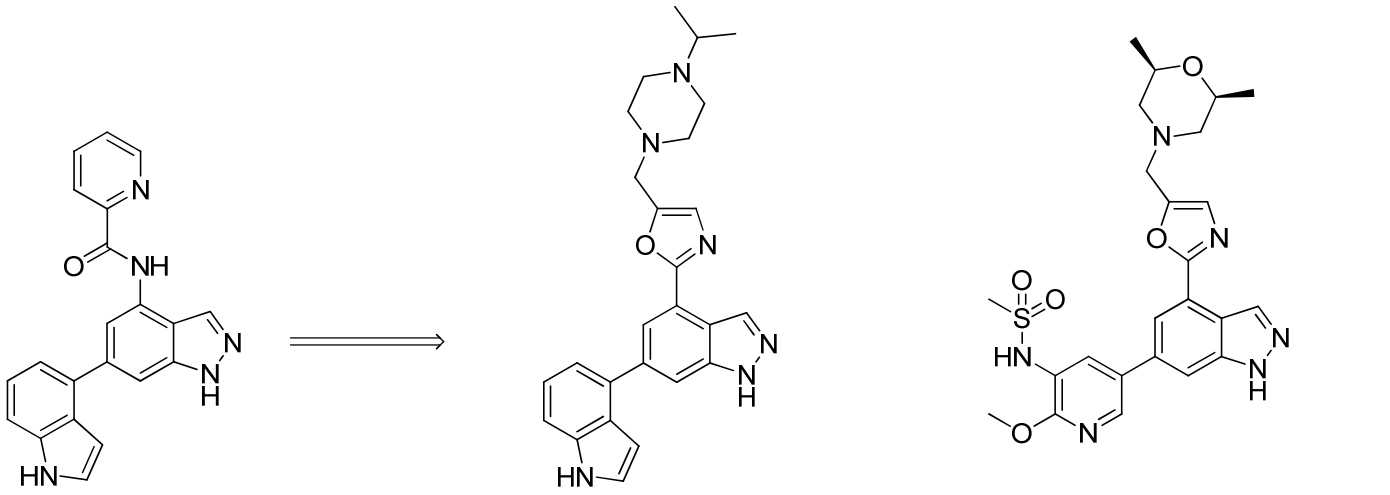

**1**

PI3Kδ p$K_i$ 7.3
~100-fold selectivity vs PI3K α, β, γ

**2**
GSK2269557

PI3Kδ p$K_i$ 9.9
>1000-fold selectivity vs PI3K α, β, γ
Rat OVA $ED_{50}$ = 67μg/kg

**3**
GSK2292767

PI3Kδ p$K_i$ 10.1
~1000-fold selectivity vs PI3K α, β, γ
Rat OVA $ED_{50}$ = 35μg/kg